Group-theoretical classification of superconducting states of strontium ruthenate

S.-O. Kaba and D. Sénéchal ⦿

Département de physique and Institut quantique, Université de Sherbrooke, Sherbrooke, Québec, Canada J1K 2R1

The possible superconducting states of strontium ruthenate (Sr_2RuO_4) are organized into irreducible representations of the point group D_{4h}, with a special emphasis on nodes occurring within the superconducting gap. Our analysis covers the cases with and without spin-orbit coupling and takes into account the possibility of interorbital pairing within a three-band, tight-binding description of Sr_2RuO_4. No dynamical treatment if performed: We are confining ourselves to a group-theoretical analysis. We nevertheless adopt an intermediate-coupling point of view by working in the orbital basis instead of the band basis. The case of uniaxial deformations, under which the point group symmetry is reduced to D_{2h}, is also covered. It turns out that nodal lines, in particular equatorial nodal lines, occur in most representations. We also highlight some results specific to multiorbital superconductivity. Among other things, we find that odd interorbital pairing allows us to combine singlet and triplet superconductivity within the same irreducible representation, that pure interorbital superconductivity leads to nodal surfaces and that the notion of nodes imposed by symmetry is not clearly defined.

I. INTRODUCTION

The problem of identifying the symmetry of the superconducting order parameter in Sr_2RuO_4 remains unsolved after more than 20 years [1–3]. Despite the impressive number of experiments that were performed on high-quality samples, there is no clear consensus on the material's superconducting state. Initial NMR Knight shift [4], neutron scattering [5], and junction [6–8] experiments seemed to point towards triplet superconductivity, although this piece of evidence is now put to question by recent studies [9]. There is also evidence for broken time reversal symmetry from muon spin resonance [10] and polar Kerr effect [11] measurements. These findings made plausible the early hypothesis of chiral triplet superconductivity [12], analogous to the A phase of ^{3}He. However, some experiments are hard to conciliate with this scenario. First, specific heat and several transport probes showed the presence of residual excitations at low temperature [13–16], most likely related to gap nodes. Secondly, the presence of an effect resembling Pauli limiting must be present in the material to explain the value of H_{c2} [17]. Lastly, no splitting of the transition was observed when applying strain to the material [18–20].

Although strontium ruthenate shares a number of common characteristics with cuprates superconductors, among which is its crystal structure [21], an important difference is its multiorbital nature. Its Fermi surface is well characterized and composed of three bands that have the character of Ru t_{2g} orbitals. It is reasonable to believe that this fact plays an important, or at least a non-negligible, role in the superconductivity of this material. The identification of a dominant band for superconductivity in Sr_2RuO_4 has not been unanimous [22–25]. Moreover, some studies suggest the possibility of important interorbital pairing in the material [26,27]. This is not too surprising when considering that strong correlations arising in the material's normal state are mainly due to Hund's coupling [28,29], which is interorbital in nature. Spin-orbit coupling, which is also known to be significant in the material [30–34], also has the effect to produce bands with mixed orbital character.

In light of this situation, we propose to reexamine the different possibilities for the order parameter of Sr_2RuO_4. A classification of possible order parameters must be done in terms of the irreducible representations of the point group symmetry of the lattice: D_{4h}, or D_{2h} when uniaxial pressure is applied. This has already been done in previous works [12,35,36], but without fully considering the multiorbital nature of the material. This means that the order parameter must be considered not only as a space- and spin-dependent function, but also as an orbital-dependent function and that the irreducible representations are to be calculated accordingly. Such a classification is important, not only in order to frame all the proposals for superconducting order parameter in a coherent picture, but also because it can provide new insights about the superconducting state. Note that we do not cover the possibility of odd-frequency pairing [27,37,38] in the present work.

In this paper, we thus introduce a complete and rigorous classification of possible superconducting states in strontium ruthenate, akin to previous classifications that were made for high-temperature and heavy-fermions superconductors [39,40]. We also highlight some features of multiorbital superconductivity that are different from what is seen in single-orbital superconductors. In particular, these considerations force us to rethink carefully the relation between the spin character of the order parameter and its parity, the possibility of combining singlet and triplet superconductivity, and the relation between order parameter symmetry and gap nodes. This classification also potentially applies to any t_{2g} superconductor sharing the symmetry group of Sr_2RuO_4.

This paper is organized as follows: In Sec. II we introduce the tight-binding model used to describe Sr_2RuO_4 and enumerate its symmetries. In Sec. III, the main section of this paper, we explain how to classify the possible superconducting states into irreducible representations of the point group D_{4h}, with an emphasis on the existence or not of nodes in the gap. Possible pairing functions are listed in Tables III, IV, and V, and generic nodes are illustrated in Fig. 3, and in Fig. 6 in the case of uniaxial deformation. We offer some discussion and conclude in Sec. IV. This work is based on the Master's thesis of one of the authors [41].

II. THE TIGHT-BINDING MODEL AND ITS SYMMETRIES

In this section we describe the Hamiltonian and its symmetries. We work in the orbital basis, not the band basis, even in reciprocal space, because it is the most appropriate to discuss symmetries at the microscopic level.

A. Hamiltonian

We will assume that Sr_2RuO_4 may be appropriately described by the following tight-binding, three-band Hamiltonian [42–44]:

$$H_0 = -t_1 \sum_{\langle \mathbf{r},\mathbf{r}'\rangle,\sigma} c^\dagger_{\mathbf{r},3,\sigma} c_{\mathbf{r}',3,\sigma} + t_2 \sum_{\langle \mathbf{r},\mathbf{r}'\rangle_2,\sigma} c^\dagger_{\mathbf{r},3,\sigma} c_{\mathbf{r}',3,\sigma} - t_3 \left[\sum_{\langle \mathbf{r},\mathbf{r}'\rangle_x,\sigma} c^\dagger_{\mathbf{r},1,\sigma} c_{\mathbf{r}',1,\sigma} + \sum_{\langle \mathbf{r},\mathbf{r}'\rangle_y,\sigma} c^\dagger_{\mathbf{r},2,\sigma} c_{\mathbf{r}',2,\sigma} \right] - \lambda \sum_{\langle \mathbf{r},\mathbf{r}'\rangle_{x+y},\sigma} (c^\dagger_{\mathbf{r},1,\sigma} c_{\mathbf{r}',2,\sigma} + \text{H.c.})$$

$$+ \lambda \sum_{\langle \mathbf{r},\mathbf{r}'\rangle_{x-y},\sigma} (c^\dagger_{\mathbf{r},1,\sigma} c_{\mathbf{r}',2,\sigma} + \text{H.c.}) + i\frac{\kappa}{2} \sum_{\mathbf{r}} \sum_{l,m,n} \varepsilon_{lmn} c^\dagger_{\mathbf{r},l,\sigma} c_{\mathbf{r},m,\sigma'} \tau^n_{\sigma\sigma'} + e \sum_{\mathbf{r},\sigma,m=1,2} c^\dagger_{\mathbf{r},m,\sigma} c_{\mathbf{r},m,\sigma} - \mu \sum_{\mathbf{r},m,\sigma} c^\dagger_{\mathbf{r},m,\sigma} c_{\mathbf{r},m,\sigma} \tag{1}$$

where $c_{\mathbf{r},m,\sigma}$ is the annihilation operator for orbital $m = 1, 2, 3$ of spin projection σ at site $\mathbf{r}$; $\langle \mathbf{r}, \mathbf{r}'\rangle$ stands for nearest-neighbor pairs and $\langle \mathbf{r}, \mathbf{r}'\rangle_2$ for second (diagonal) neighbors; $\langle \mathbf{r}, \mathbf{r}'\rangle_x$ stands for nearest-neighbor pairs in the x direction, and likewise for the y, $x + y$, and $x - y$ directions. The κ term is a spin-orbit coupling, where $\tau^{1,2,3}$ are the Pauli matrices and ε_{lmn} the Levi-Civita antisymmetric symbol. Note that the chosen labeling of the three orbitals ($d_{yz} \to 1$, $d_{xz} \to 2$, $d_{xy} \to 3$) is important in this expression. Figure 1 illustrates the orbitals and hopping terms involved ($t_{1,2,3}$ and λ). On that figure, the three orbitals have been separated vertically for clarity. The first two orbitals (1 and 2) are separated by an energy e from the third.

The interaction terms include local Coulomb interactions U (intraorbital) and U' (interorbital), as well as Hund couplings J and J':

$$H_1 = \sum_{\mathbf{r}} \left\{ U \sum_l n_{\mathbf{r},l,\uparrow} n_{\mathbf{r},l,\downarrow} + \sum_{m\neq m'} \left[U' \sum_{\sigma,\sigma'} n_{\mathbf{r},m,\sigma} n_{\mathbf{r},m',\sigma'} + \frac{J}{2} \sum_{\sigma,\sigma'} c^\dagger_{\mathbf{r},m,\sigma} c^\dagger_{\mathbf{r},m',\sigma'} c_{\mathbf{r},m,\sigma'} c_{\mathbf{r},m',\sigma} + \frac{J'}{2} \sum_{\sigma\neq\sigma'} c^\dagger_{\mathbf{r},m,\sigma} c^\dagger_{\mathbf{r},m,\sigma'} c_{\mathbf{r},m',\sigma'} c_{\mathbf{r},m',\sigma} \right] \right\} \tag{2}$$

Ultimately we are interested in studying the full interacting Hamiltonian in the framework of an appropriate strong- or intermediate-coupling approach. This we reserve for future work, and for the moment we are just pointing out that the interaction H_1 has the same point-group symmetries as the noninteracting part (see next subsection). However, the strongly correlated nature of Sr_2RuO_4, evident from the important effective mass renormalizations [1,45], justifies using the orbital basis in our symmetry analysis.

The noninteracting Hamiltonian (1) can be expressed in momentum space:

$$H_0 = \sum_{m,m',\sigma,\sigma',\mathbf{k}} c^\dagger_{\mathbf{k},m,\sigma} \mathcal{H}_0(\mathbf{k})_{m\sigma,m'\sigma'} c_{\mathbf{k},m',\sigma'} \tag{3}$$

with the 6×6 matrix

$$\mathcal{H}_0(\mathbf{k}) = \begin{pmatrix} e - \mu - 2t_3 \cos k_y & \frac{i}{2}\kappa + \lambda_\mathbf{k} & 0 & 0 & 0 & -\frac{1}{2}\kappa \\ -\frac{i}{2}\kappa + \lambda_\mathbf{k} & e - \mu - 2t_3 \cos k_x & 0 & 0 & 0 & \frac{i}{2}\kappa \\ 0 & 0 & t_{1,\mathbf{k}} + t_{2,\mathbf{k}} - \mu & \frac{1}{2}\kappa & -\frac{i}{2}\kappa & 0 \\ 0 & 0 & \frac{1}{2}\kappa & e - \mu - 2t_3 \cos k_y & -\frac{i}{2}\kappa + \lambda_\mathbf{k} & 0 \\ 0 & 0 & \frac{i}{2}\kappa & \frac{i}{2}\kappa + \lambda_\mathbf{k} & 0 & 0 \\ -\frac{1}{2}\kappa & -\frac{i}{2}\kappa & 0 & 0 & 0 & t_{1,\mathbf{k}} + t_{2,\mathbf{k}} - \mu \end{pmatrix} \tag{4}$$

where we have introduced

$$t_{1,\mathbf{k}} = -2t_1(\cos k_x + \cos k_y) \tag{5}$$

$$t_{2,\mathbf{k}} = 4t_2 \cos k_x \cos k_y \tag{6}$$

$$\lambda_\mathbf{k} = -4\lambda \sin k_x \sin k_y. \tag{7}$$

The degrees of freedom are placed in the following order:

$$(1\uparrow, 2\uparrow, 3\uparrow, 1\downarrow, 2\downarrow, 3\downarrow). \tag{8}$$

Upon diagonalizing the matrix $\mathcal{H}_0(\mathbf{k})$ when $\kappa = 0$, one recovers three bands: The d_{xy} orbital forms a band of its own labeled γ; the other two orbitals hybridize because of the λ term and form two bands labeled α and β. The associated Fermi surfaces are illustrated in red in Fig. 2. However, symmetries are more easily described in terms of the original
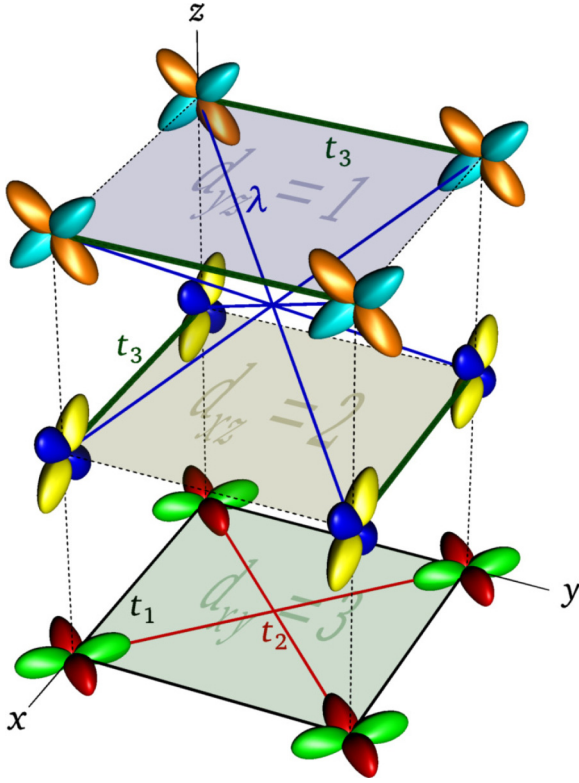
FIG. 1. Schematic view of the SRO unit cell. The three orbitals have been vertically separated for clarity (the model considered is purely two dimensional). The labels 1,2,3 correspond, respectively, to the d_{yz}, d_{xz}, and d_{xy} orbitals. The different hopping terms ($t_{1,2,3}$ and λ) are illustrated.

FIG. 2. Illustration of the possible nodes in pairing functions. In red: the normal state Fermi surface, with the band labels α, β, and γ. In Tables III, IV, and V, the + sign stands for the intersection of any of these surfaces with horizontal/vertical axes (blue dots), including zone boundaries. The × sign stands for the intersection of either of these surfaces with diagonal axes (open black dots). The −, | and ⟍ signs will stand for the intersection with the horizontal, vertical, and northwest diagonals only.

orbitals, and therefore we will stick to the orbital description in the remainder of this paper.

Throughout this work, we use the following values of the band parameters: $t_1 = 1$ (the unit of energy), $t_2 = 0.4$, $t_3 = 1.25$, $\lambda = -0.1$, $e = 0.1$, and $\mu = 1.5$. These values are compatible with the ones used in the literature [25,44,46–48]. When present, the spin-orbit coupling κ is set to 0.2; this value was chosen somewhat arbitrarily, in order to have a visible impact on the dispersion relation (or Fermi surface).

B. Symmetries

The Hamiltonian $H = H_0 + H_1$ has the following symmetries:

(1) A mirror symmetry σ_x with respect to the yz plane; this reflection changes the signs of orbitals 2 and 3.

(2) A mirror symmetry σ_y with respect to the xz plane; this reflection changes the signs of orbitals 1 and 3.

(3) A $\pi/2$ rotation C_4 around the z axis, together with the following exchange of orbitals: $d_{xz} \to d_{yz}$ and $d_{yz} \to -d_{xz}$ orbitals. The d_{xy} orbital changes sign under this rotation.

(4) Even though the model is two dimensional, we could imagine a reflection σ_z with respect to the xy plane that changes the signs of orbitals 2 and 3. Strictly speaking, this is an internal symmetry in the context of a two-dimensional model, but it will be relevant when classifying the superconducting pairing functions.
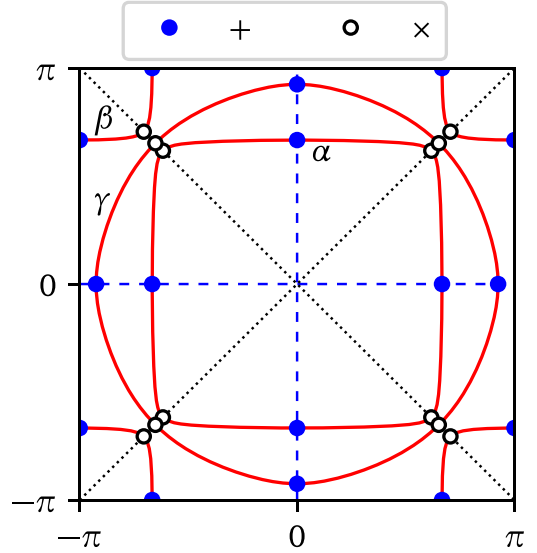
Operations 1–4 above generate the 16-element point group D_{4h}.

(5) If $\kappa = 0$, a simultaneous rotation of all spins. Otherwise these rotations are not independent of the spatial symmetries (see below).

(6) Time reversal.

(7) A $U(1)$ symmetry leading to the conservation of the total number of electrons in all three orbitals.

(8) A Z_2 symmetry leading to the separate conservation of the parity (odd or even) of the number of electrons (i) in the d_{xy} orbitals and (ii) in the d_{yz} and d_{xz} orbitals. Indeed, were it not for the interactions, the number of electrons would be separately conserved in the d_{xy} on one hand and in the set d_{yz}, d_{xz} on the other hand. The Hund coupling, however, allows pair hopping between these two sets.

(9) Translation symmetry on the lattice.

Let us consider a symmetry transformation g acting on space. In the absence of spin-orbit coupling, such a transformation does not affect spin and its effect on the annihilation operator $c_{\mathbf{r},m,\sigma}$ is the following:

$$c_{\mathbf{r},m,\sigma} \to c'_{\mathbf{r},m,\sigma} = \sum_{m'} U_{mm'}(g) c_{g\mathbf{r},m',\sigma}, \qquad (9)$$

where $g\mathbf{r}$ is the mapping of site $\mathbf{r}$ under the spatial symmetry transformation and $U(g)$ is a 3×3 matrix. On the other hand, when $\kappa \neq 0$, such a transformation must be accompanied by a spin rotation:

$$c_{\mathbf{r},m,\sigma} \to c'_{\mathbf{r},m,\sigma} = \sum_{m',\sigma'} S_{\sigma\sigma'}(g) U_{mm'}(g) c_{\mathbf{r}',m',\sigma'}. \qquad (10)$$

TABLE I. Generators of the point group D_{4h}. U is the orbital part, S the spin part (in the case of spin-orbit coupling) and R the associated rotation of the **d** vector.

Generator	U	S	R
C_4	$\begin{pmatrix} 0 & 1 & 0 \\ -1 & 0 & 0 \\ 0 & 0 & -1 \end{pmatrix}$	$\begin{pmatrix} \frac{1+i}{\sqrt{2}} & 0 \\ 0 & \frac{1-i}{\sqrt{2}} \end{pmatrix}$	$\begin{pmatrix} 0 & 1 & 0 \\ -1 & 0 & 0 \\ 0 & 0 & 1 \end{pmatrix}$
σ_x	$\begin{pmatrix} 1 & 0 & 0 \\ 0 & -1 & 0 \\ 0 & 0 & -1 \end{pmatrix}$	$\begin{pmatrix} 0 & i \\ i & 0 \end{pmatrix}$	$\begin{pmatrix} 1 & 0 & 0 \\ 0 & -1 & 0 \\ 0 & 0 & -1 \end{pmatrix}$
σ_y	$\begin{pmatrix} -1 & 0 & 0 \\ 0 & 1 & 0 \\ 0 & 0 & -1 \end{pmatrix}$	$\begin{pmatrix} 0 & 1 \\ -1 & 0 \end{pmatrix}$	$\begin{pmatrix} -1 & 0 & 0 \\ 0 & 1 & 0 \\ 0 & 0 & -1 \end{pmatrix}$
σ_z	$\begin{pmatrix} -1 & 0 & 0 \\ 0 & -1 & 0 \\ 0 & 0 & 1 \end{pmatrix}$	$\begin{pmatrix} i & 0 \\ 0 & -i \end{pmatrix}$	$\begin{pmatrix} -1 & 0 & 0 \\ 0 & -1 & 0 \\ 0 & 0 & 1 \end{pmatrix}$

Under this more general transformation, the spin-orbit term becomes

$$i\frac{\kappa}{2} \sum_{\mathbf{r}} \sum_{l,m,n} \varepsilon_{l'm'n} U_{l'l}^* U_{m'm} c_{\mathbf{r},l,\sigma}^\dagger c_{\mathbf{r},m,\sigma'} S_{\alpha\sigma}^* S_{\alpha'\sigma'} \tau_{\alpha\alpha'}^n. \quad (11)$$

The spin rotation matrix S must belong to a spinorial representation of the group such that

$$S^\dagger \tau^n S = R_{nn'} \tau^{n'}$$
$$\varepsilon_{l'm'n} U_{l'l}^* U_{m'm} = R_{nn'}^{-1} \varepsilon_{lmn'} \quad (12)$$

in order for the spin-orbit term to be invariant.

The appropriate matrices U and S, as well as the resulting rotation matrix R of Eq. (12), are listed in Table I for the four generators C_4, σ_x, σ_y, and σ_z. One checks that these matrices guarantee the invariance of the complete Hamiltonian under these transformations; in the absence of spin-orbit coupling, one can simply ignore the last two columns. These three transformations generate a group isomorphic to D_{4h}, which as 16 elements and 10 irreducible representations (or *irreps*, as we will call them from now on). Its character table is given in Table II. The precise form of the U matrices takes into account the change of sign of the d orbitals under spatial transformations.

The symmetry operations described above would have a different form if expressed in the band basis instead of the orbital basis. Specifically, the annihilation operator $d_a(\mathbf{k})$ of an electron in band a can be expressed in terms of its orbital basis equivalent $c_{\mathbf{k},m,\sigma}$ as

$$d_{\mathbf{k},a}(\mathbf{k}) = \sum_{m,\sigma} V_{a,m\sigma}(\mathbf{k}) c_{\mathbf{k},m,\sigma} \quad (13)$$

where $V_{a,m\sigma}(\mathbf{k})$ is a momentum-dependent unitary matrix obtained from diagonalizing $\mathcal{H}_0(\mathbf{k})$ in Eq. (4). The index a takes six values, the bands being pairwise degenerate in the absence of spin-orbit coupling. The transformation of $d_a(\mathbf{k})$ under a group element g reads

$$d_a'(\mathbf{k}) = \sum_b \tilde{U}_{ab}(g,\mathbf{k}) d_b(g\mathbf{k}) \quad (14)$$

where $g\mathbf{k}$ is the image of $\mathbf{k}$ under the point group transformation g and

$$\tilde{U}_{ab}(g,\mathbf{k}) = \sum_{m,m',\sigma,\sigma'} V_{a,m\sigma}(\mathbf{k}) V_{b,m'\sigma'}^*(\mathbf{k}) S_{\sigma\sigma'}(g) U_{mm'}(g). \quad (15)$$

The matrix $\tilde{U}_{ab}(g,\mathbf{k})$ depends on momentum $\mathbf{k}$, whereas the matrices $S_{\sigma\sigma'}(g)$ and $U_{mm'}(g)$ are constant. Hence the orbital basis makes the group-theoretical analysis much simpler.

III. SYMMETRIES OF THE ORDER PARAMETER

A. General considerations

A general superconducting order parameter may be expressed in real space as

$$\Delta_{\mathbf{r},m,\sigma;\mathbf{r}',m',\sigma'} = \langle c_{\mathbf{r},m,\sigma} c_{\mathbf{r}',m',\sigma'} \rangle. \quad (16)$$

Assuming translation symmetry, this order parameter depends on the difference $\mathbf{r} - \mathbf{r}'$ and is diagonal in $\mathbf{k}$ space:

$$\Delta_{m,\sigma;m',\sigma'}(\mathbf{k}) = \langle c_{m,\sigma}(\mathbf{k}) c_{m',\sigma'}(-\mathbf{k}) \rangle. \quad (17)$$

The Pauli principle imposes antisymmetry under the exchange of the quantum numbers of the pair:

$$\Delta_{m,\sigma;m',\sigma'}(\mathbf{k}) = -\Delta_{m',\sigma';m,\sigma}(-\mathbf{k}). \quad (18)$$

In the remainder of this paper, the words *symmetric* and *antisymmetric* will refer to the properties of various parts of

TABLE II. Character table of D_{4h}, with a list of the simplest (i.e., lowest degree) singlet and triplet pairing functions for a single-band model without spin-orbit representation. Note that we distinguish g-type representations, which are even under inversion (i), from u-type representations, which are odd under inversion.

	E	$2C_4$	C_2	$2C_2'$	$2C_2''$	i	$2S_4$	σ_z	$\sigma_{x,y}$	$\sigma_{d,d'}$	Pairing function	Nodes	Spin
A_{1g}	1	1	1	1	1	1	1	1	1	1	1	none	0
A_{2g}	1	1	1	-1	-1	1	1	1	-1	-1	$xy(x^2-y^2)$	eightfold	0
B_{1g}	1	-1	1	1	-1	1	-1	1	1	-1	x^2-y^2	fourfold diagonal	0
B_{2g}	1	-1	1	-1	1	1	-1	1	-1	1	xy	fourfold	0
E_g	2	0	-2	0	0	2	0	-2	0	0	$z(x,y)$	equator, twofold	0
A_{1u}	1	1	1	1	1	-1	-1	-1	-1	-1	$xyz(x^2-y^2)$	equator, eightfold	1
A_{2u}	1	1	1	-1	-1	-1	-1	-1	1	1	z	equator	1
B_{1u}	1	-1	1	1	-1	-1	1	-1	-1	1	xyz	equator, fourfold	1
B_{2u}	1	-1	1	-1	1	-1	1	-1	1	-1	$z(x^2-y^2)$	equator, fourfold diagonal	1
E_u	2	0	-2	0	0	-2	0	2	0	0	(x,y)	twofold (R) or none (C)	1

the pairing function with respect to the exchange of the two electrons.

A general order parameter function (or pairing function) can be expressed as a linear combination of basis functions. We can use a basis made of tensor products of position-dependent, orbital-dependent, and spin-dependent factors:

$$\Delta_{m,\sigma;m',\sigma'}(\mathbf{k}) = \sum_{\mu\nu\rho} C_{\mu\nu\rho} f^\mu(\mathbf{k}) O^\nu_{mm'} S^\rho_{\sigma\sigma'} . \qquad (19)$$

The spin part of the pairing function is generally described by the so-called **d** vector, defined as follows:

$$S_{\sigma\sigma'} = id_\rho(\tau_\rho\tau_2)_{\sigma\sigma'} = d_\rho\hat{\mathbf{d}}_\rho . \qquad (20)$$

The three components $d_{x,y,z}$ form the symmetric, triplet part of the spin part of the pairing function, whereas the antisymmetric, singlet part is represented by the zeroth component d_0 (the set of Pauli matrices $\tau_{1,2,3}$ is augmented by the identity matrix τ_0). Under a rotation in spin space, the three-vector **d** transforms as a pseudovector (i.e., invariant under inversion), and d_0 behaves like a pseudoscalar (it changes sign under inversion). In the presence of spin-orbit coupling, d_z falls into the A_{2g} representation and (d_x, d_y) into E_g, whereas d_0 corresponds to A_{1g}.

Likewise, we will define the following 3×3 matrices to serve as a basis in orbital space:

$$\hat{\mathbf{a}}_x = \begin{pmatrix} 1 & 0 & 0 \\ 0 & 0 & 0 \\ 0 & 0 & 0 \end{pmatrix} \quad \hat{\mathbf{b}}_x = \begin{pmatrix} 0 & 0 & 0 \\ 0 & 0 & 1 \\ 0 & 1 & 0 \end{pmatrix} \quad \hat{\mathbf{c}}_x = \begin{pmatrix} 0 & 0 & 0 \\ 0 & 0 & 1 \\ 0 & -1 & 0 \end{pmatrix}$$

$$\hat{\mathbf{a}}_y = \begin{pmatrix} 0 & 0 & 0 \\ 0 & 1 & 0 \\ 0 & 0 & 0 \end{pmatrix} \quad \hat{\mathbf{b}}_y = \begin{pmatrix} 0 & 0 & 1 \\ 0 & 0 & 0 \\ 1 & 0 & 0 \end{pmatrix} \quad \hat{\mathbf{c}}_y = \begin{pmatrix} 0 & 0 & 1 \\ 0 & 0 & 0 \\ -1 & 0 & 0 \end{pmatrix}$$

$$\hat{\mathbf{a}}_z = \begin{pmatrix} 0 & 0 & 0 \\ 0 & 0 & 0 \\ 0 & 0 & 1 \end{pmatrix} \quad \hat{\mathbf{b}}_z = \begin{pmatrix} 0 & 1 & 0 \\ 1 & 0 & 0 \\ 0 & 0 & 0 \end{pmatrix} \quad \hat{\mathbf{c}}_z = \begin{pmatrix} 0 & 1 & 0 \\ -1 & 0 & 0 \\ 0 & 0 & 0 \end{pmatrix} .$$

A general matrix acting on orbital space may then be expressed via three vectors **a**, **b**, and **c** as

$$O_{mn} = \mathbf{a} \cdot \hat{\mathbf{a}}_{mn} + \mathbf{b} \cdot \hat{\mathbf{b}}_{mn} + \mathbf{c} \cdot \hat{\mathbf{c}}_{mn} . \qquad (21)$$

The components of these vectors, like the annihilation operators $c_{\mathbf{r},m,\sigma}$, will be labeled using indices $m = x, y, z$, corresponding, respectively, to the three orbitals d_{yz}, d_{xz}, and d_{xy}, also numbered 1,2,3 in Fig. 1. Clearly the **a** and **b** vectors describe symmetric orbital parts of the pairing function, and **c** antisymmetric orbital parts. The advantage of defining the vectors **a**, **b**, and **c** lies in their transformation properties: The combinations a_z and $a_x + a_y$ belong to the A_{1g} representation, and $a_x - a_y$ to B_{1g}. The component b_z belongs to B_{2g}, whereas c_z belongs to A_{2g}. Finally, the pairs (b_x, b_y) and (c_x, c_y) both belong to E_g. Said differently, the **a** vector transforms like the functions (x^2, y^2, z^2), the **b** vector like the functions (yz, xz, xy), and the **c** vector like a pseudovector.

As for the spatial part of the pairing function, it will be described by multinomials in x, y, z, which in fact stand for the components k_x, k_y, k_z of the wave vector. The three linear functions $\{x, y, z\}$ form a "vector" representation of D_{4h}, which is obviously reducible: z belongs to the A_{2u}

representation and (x, y) form the two-component E_u representation. By taking symmetrized tensor products of this reducible representation repeatedly with itself, one finds reducible representations for quadratic, cubic, quartic functions, and so on. The even-degree functions are symmetric under inversion (which corresponds here to exchanging the spatial quantum numbers), whereas the odd-degree functions are antisymmetric.

The coefficient $C_{\mu\nu\rho}$ of Eq. (19) will therefore be expressed in terms of components of the **d**-vector for the spin index ρ, components of the **a**, **b**, and **c** vectors for the orbital index ν, and multinomial functions of x, y, z for the spatial part. For instance, the pairing function $\hat{\mathbf{c}}_z\hat{\mathbf{d}}_z(x^2 - y^2)$, which appears below in Table V under the B_{1g} representation, represents a spin triplet $(|\uparrow\downarrow\rangle + |\downarrow\uparrow\rangle)$ with an antisymmetric orbital combination of d_{xz} and d_{yz} (because of $\hat{\mathbf{c}}_z$), and a d-wave-like spatial part. The product $\hat{\mathbf{c}}_z\hat{\mathbf{d}}_z$ is a tensor product of a 3×3 matrix acting in orbital space ($\hat{\mathbf{c}}_z$) with a 2×2 matrix acting in spin space ($\hat{\mathbf{d}}_z$), so that the overall pairing function in this case is a 6×6 matrix.

Note that the pairing function may also be expressed in the band basis:

$$\tilde{\Delta}_{ab}(\mathbf{k}) = \sum_{m,m',\sigma,\sigma'} V_{a,m\sigma}(\mathbf{k}) V_{b,m'\sigma'}(-\mathbf{k}) \Delta_{m,\sigma;m',\sigma'}(\mathbf{k}) \qquad (22)$$

where the matrix $V_{a,m\sigma}(\mathbf{k})$ was introduced in Eq. (13). Interorbital pairing ($m \neq m'$) will in general contribute to intraband pairing ($a = b$) and vice versa, in a momentum-dependent way. Let us stress again that, from a microscopic point of view appropriate in an intermediate- to strong-coupling context, the orbital basis allows for a simple description of symmetries.

B. Landau theory

We assume that the pattern of symmetry breaking occurs within the framework of the Landau theory of phase transitions. A generic superconducting order parameter may be decomposed on a basis of possible pairing functions $\hat{\Delta}_\mu$, i.e., $\Delta = \sum_\mu \psi_\mu \hat{\Delta}_\mu$, and the Landau free energy functional is a power expansion in terms of the coefficients ψ_μ:

$$f[\psi] = a_{\mu\nu}(T)\psi^*_\mu \psi_\nu + b_{\mu\nu\rho\lambda}(T)\psi^*_\mu \psi^*_\nu \psi_\rho \psi_\lambda + \cdots \qquad (23)$$

where the ellipsis stands for gradient and higher-degree terms, and T is the temperature.

Organizing the basis functions $\hat{\Delta}_\mu$ according to irreps of the point group makes the matrix $a(T)$ block diagonal: $a(T) = \bigoplus_r a^{(r)}(T)$, i.e., it has no matrix elements between functions belonging to different irreps. Within each representation, the matrix $a^{(r)}(T)$ may be diagonalized, and at some point upon lowering T one of its eigenvalues, initially all positive, may change sign, which signals the superconducting phase transition and a minimum of $f[\psi]$ at $\psi \neq 0$. This is going to first occur in one of the representations and will define the symmetry character of the superconducting state. Nothing forbids competing minima, and hence additional phase transitions, to appear at lower temperatures. These transitions should be detectable, for instance by specific heat measurements. None has been seen in Sr_2RuO_4 [1,3], and therefore we will assume a single symmetry breaking pattern in this work.

If the transition occurs in the A_{1g} representation, then the only broken symmetry is the $U(1)$ of gauge invariance. In any other irrep, the point group D_{4h} is broken as well, but not completely: The minimum $\psi^\star$ leaves a subgroup of D_{4h} invariant. For instance, in the B_{1g} representation, the superconducting state is effectively a distortion that breaks D_{4h} down to the group D_{2h} as described in Sec. III G below, and it happens that all basis functions of B_{1g} are invariant under this subgroup. It is noteworthy that for a group like D_{4h}, which only has one-dimensional and two-dimensional chiral-like irreps (E_g and E_u), this invariant subgroup only depends on the irrep of the solution, i.e., it is the same for all basis functions within that irrep. This means that, in a given state of broken symmetry, all basis functions of a given irrep may *a priori* contribute to the total (or combined) pairing function.

Time reversal (TR) symmetry may only occur when the minimum $\psi^\star$ is degenerate, and this will occur only within a two-dimensional representation (E_g or E_u). In those cases, the complex combination $(1, i)$ of the two basis functions defines a broken TR state, with the conjugate combination $(1, -i)$ being the time-reversed state. Other TR broken states could only occur when two solutions belonging to different representations happen to have the same energy, which implies a second phase transition as mentioned above. We exclude that possibility.

C. Quasiparticle dispersion

In order to identify nodes, or other elementary properties of the superconducting state, one must compute the quasiparticle dispersion; this is done at the mean-field level. The pairing function $\Delta_{\mathbf{k}}$ is a 6×6 matrix. It appears in the mean-field Hamiltonian as

$$F = \sum_{m,m',\sigma,\sigma',\mathbf{k}} c_{\mathbf{k},m,\sigma} \Delta(\mathbf{k})_{m\sigma,m'\sigma'} c_{-\mathbf{k},m',\sigma'} + \text{H.c.} \quad (24)$$

The normal and anomalous part of the Hamiltonian are put together via the Nambu formalism, in which we introduce a 12-component spinor at a given wave vector $\mathbf{k}$ [49]:

$$\Psi_{\mathbf{k}} = (c_{\mathbf{k},m,\sigma}, c^\dagger_{-\mathbf{k},m,\sigma}) \quad (m = 1, 2, 3; \ \sigma = \uparrow, \downarrow). \quad (25)$$

The combined Hamiltonian takes the following form:

$$H = \sum_{\mathbf{k}} \Psi^\dagger_{\mathbf{k}} \mathcal{H}(\mathbf{k}) \Psi_{\mathbf{k}} \quad (26)$$

with the 12×12 matrix

$$\mathcal{H}(\mathbf{k}) = \begin{pmatrix} \mathcal{H}_0(\mathbf{k}) & \Delta(\mathbf{k}) \\ \Delta^\dagger(\mathbf{k}) & -\mathcal{H}_0^*(\mathbf{k}) \end{pmatrix}. \quad (27)$$

The eigenvalues of $\mathcal{H}(\mathbf{k})$ occur in pairs of opposite signs and provide the dispersion relation of the quasiparticles. Nodes are found by looking for the zeros of these eigenvalues.

D. No spin orbit coupling

In the following, we will construct possible pairing functions $\Delta(\mathbf{k})$ organized according to irreps of the point group D_{4h}, keeping the spatial part as simple as possible. The construction of pairing functions is simpler in the absence of spin-orbit coupling, because the spin part always factorizes

from the rest and is either a singlet or a triplet. One can then concentrate on the construction of the spatial-orbital part, which must be symmetric in the singlet case, and antisymmetric otherwise.

This construction can be automated as follows: One constructs a 3×3 matrix representation $U_{mm'}(g)$ of each of the 16 elements g of D_{4h} acting in orbital space, by combining the generators of Table I. The symmetrized and antisymmetrized tensor products of this representation with itself are then constructed:

$$\mathcal{S} U(g) \otimes U(g) \quad \text{and} \quad \mathcal{A} U(g) \otimes U(g) \quad (28)$$

($\mathcal{S}$ and $\mathcal{A}$ are the symmetrizer and antisymmetrizer, respectively). The tensor products of these orbital representations with the spatial representations of a given degree in (x, y, z) are constructed next. The resulting higher-dimensional representation $R(g)$ can then be projected onto irreps or D_{4h} with the help of projection operators:

$$P^{(r)} = \frac{d^{(r)}}{|G|} \sum_{g \in G} \chi_g^{(r)*} R(g) \quad (29)$$

where G stands for the point group (here D_{4h}), the sum is over the $|G|$ group elements g, and $\chi^{(r)}$ is the character of the irrep r (according to Table II). This procedure is done using a combination of numerical and symbolic computations in the Python language.

Among the states selected by the projection operator, some involve only the vector $\mathbf{a}$ and therefore describe intraorbital pairing. Those involving the components of $\mathbf{b}$ describe interorbital pairing that is symmetric in orbital (and consequently associated to a symmetric spatial part for singlets and antisymmetric spatial part for triplets). Those involving the components of $\mathbf{c}$ describe interorbital pairing that is antisymmetric in orbital (and consequently associated to an antisymmetric spatial part for singlets and symmetric spatial part for triplets).

Table III lists the singlet pairing functions found in this way. They are enumerated according to irrep and, within each irrep, according to the type of orbital pairing:

(1) d_{xy}: intraorbital pairing within the d_{xy} orbital, forming the so-called γ band.

(2) d_{xz}, d_{yz}: intraorbital pairing within the d_{yz} or d_{xz} orbital.

(3) d_{xz}/d_{yz}: interorbital pairing between the d_{yz} and d_{xz} orbitals.

(4) d_{xy}/d_{xz}, d_{xy}/d_{yz}: interorbital pairing between d_{xy} and d_{yz} orbitals, or between d_{xy} and d_{xz} orbitals.

For the sake of illustrating each type of orbital pairing, we have carried the construction of spatial functions to a degree sufficient to display all cases, but displaying only the lowest degree in each. Column 4 of Table III shows the pairing function as a function of orbital vector and coordinates (x, y, z), or equivalently (k_x, k_y, k_z). In order to represent lattice quantities in the full Brillouin zone and to identify nodes in the dispersion, we perform the following substitutions for x:

$$x \to \sin k_x \qquad x^2 \to 1 - \cos k_x \quad (30)$$

and likewise for y and z. Such a substitution would allow us to provide a real-space description of pairing. For instance,

TABLE III. List of singlet pairing functions (no spin-orbit coupling). Functions are arranged according to D_{4h} representations and type of interorbital pairing: intraorbital (d_{xy}, d_{xz}, or d_{yz}) or interorbital (d_{xy}/d_{xz}, d_{xy}/d_{yz}, d_{xy}/d_{yz}, d_{xz}/d_{yz}). The notation for the nodes is the following: α, β, and γ refer to the normal state Fermi surface sheets (see Fig. 2); when appearing alone, it means that the whole sheet is a nodal surface. They can be hybridized, hence the notation ($\beta\gamma$), etc. When appearing next to a symbol ($+$, $|$, $-$, $\times$, $\searrow$), then the node is the intersection of that sheet with particular lines: $+$ stands for horizontal and vertical axes at 0 and $\pm\pi$; $-$ and $|$ stand for horizontal and vertical lines only, whereas $\times$ stands for the diagonals and $\searrow$ for the north-west diagonal only. Commas separate different nodal lines or surfaces present. The combined nodes are obtained in mixing the different functions in a given representation. For functions that do not involve z, the nodes are k_z independent in our approximation that neglects hopping in the z direction. For functions that depend on z, the nodes indicated here are computed at $k_z = \pi/2$; in those cases the pairing function vanishes at $k_z = 0$ and the nodes there coincide with the complete Fermi surface.

Irrep	Combined nodes	Orbital mixing	Pairing function	Nodes
A_{1g}	none	d_{xy}	$\hat{\mathbf{a}}_x$	α, β
		d_{xz}, d_{yz}	$\hat{\mathbf{a}}_x + \hat{\mathbf{a}}_y$	γ
		d_{xz}/d_{yz}	$\hat{\mathbf{b}}_z xy$	$\gamma, +\alpha, +\beta$
		$d_{xy}/d_{xz}, d_{xy}/d_{yz}$	$z(\hat{\mathbf{b}}_x y - \hat{\mathbf{b}}_y x)$	$(\alpha\beta\gamma)$
A_{2g}	$+\gamma, +\beta$	d_{xy}	$\hat{\mathbf{a}}_z xy(x^2 - y^2)$	$\alpha, \beta, + \times \gamma$
		d_{xz}, d_{yz}	$xy(\hat{\mathbf{a}}_x - \hat{\mathbf{a}}_y)$	$\gamma, + \times \alpha, +\beta$
		d_{xz}/d_{yz}	$\hat{\mathbf{b}}_z(x^2 - y^2)$	$\gamma, + \times \alpha, + \times \beta$
		$d_{xy}/d_{xz}, d_{xy}/d_{yz}$	$z(\hat{\mathbf{b}}_x x + \hat{\mathbf{b}}_y y)$	α, β, γ
B_{1g}	$\times\beta$	d_{xy}	$\hat{\mathbf{a}}_z(x^2 - y^2)$	$\times\gamma, \alpha, \beta$
		d_{xz}, d_{yz}	$\hat{\mathbf{a}}_x - \hat{\mathbf{a}}_y$	$\gamma, \times\alpha, \times\beta$
		d_{xz}/d_{yz}	$\hat{\mathbf{b}}_z xy(x^2 - y^2)$	$\gamma, + \times \alpha, + \times \beta$
		$d_{xy}/d_{xz}, d_{xy}/d_{yz}$	$z(\hat{\mathbf{b}}_x y + \hat{\mathbf{b}}_y x)$	$(\alpha\gamma), \beta$
B_{2g}	$+\alpha, +\gamma, +\beta$	d_{xy}	$\hat{\mathbf{a}}_z xy$	$\alpha, \beta, +\gamma$
		d_{xz}, d_{yz}	$xy(\hat{\mathbf{a}}_x + \hat{\mathbf{a}}_y)$	$\gamma, +\alpha, +\beta$
		d_{xz}/d_{yz}	$\hat{\mathbf{b}}_z$	$\gamma, +\alpha, +\beta$
		$d_{xy}/d_{xz}, d_{xy}/d_{yz}$	$z(\hat{\mathbf{b}}_x x - \hat{\mathbf{b}}_y y)$	$\alpha, (\beta, \gamma)$
E_g	$\beta, (\alpha\gamma) : (\alpha\beta\gamma) : \beta, (\alpha\gamma)$	d_{xy}	$\hat{\mathbf{a}}_z z(x, y)$	$\alpha, \beta, |\gamma : \alpha, \beta, \searrow\gamma : \alpha, \beta$
		d_{xz}, d_{yz}	$z(\hat{\mathbf{a}}_x x, \hat{\mathbf{a}}_y y)$	$+\alpha, +\beta, \gamma : + \times \alpha, + \times \beta, \gamma : +\alpha, +\beta, \gamma$
			$z(\hat{\mathbf{a}}_x y, \hat{\mathbf{a}}_y x)$	$-\alpha, -\beta, \gamma : \searrow\alpha\searrow\beta, \gamma : \gamma$
		d_{xz}/d_{yz}	$\hat{\mathbf{b}}_z z(x, y)$	$+\alpha, +\beta, \gamma : +\alpha, +\beta, \gamma : +\alpha, +\beta, \gamma$
		$d_{xy}/d_{xz}, d_{xy}/d_{yz}$	$(\hat{\mathbf{b}}_x, \hat{\mathbf{b}}_y)$	$\beta, (\alpha\gamma) : (\alpha\beta\gamma) : \beta, (\alpha\gamma)$
A_{1u}	$\beta, (\alpha\gamma)$	d_{xz}/d_{yz}	$\hat{\mathbf{c}}_z z$	α, β, γ
		$d_{xy}/d_{xz}, d_{xy}/d_{yz}$	$\hat{\mathbf{c}}_x x + \hat{\mathbf{c}}_y y$	$\beta, (\alpha\gamma)$
A_{2u}	$\alpha, (\beta\gamma)$	d_{xz}/d_{yz}	$\hat{\mathbf{c}}_z xyz(x^2 - y^2)$	α, β, γ
		$d_{xy}/d_{xz}, d_{xy}/d_{yz}$	$\hat{\mathbf{c}}_x y - \hat{\mathbf{c}}_y x$	$(\alpha\beta\gamma)$
B_{1u}	$\alpha, (\beta\gamma)$	d_{xz}/d_{yz}	$\hat{\mathbf{c}}_z z(x^2 - y^2)$	α, β, γ
		$d_{xy}/d_{xz}, d_{xy}/d_{yz}$	$\hat{\mathbf{c}}_x x - \hat{\mathbf{c}}_y y$	$\alpha, (\beta\gamma)$
B_{2u}	$\beta, (\alpha\gamma)$	d_{xz}/d_{yz}	$\hat{\mathbf{c}}_z xyz$	α, β, γ
		$d_{xy}/d_{xz}, d_{xy}/d_{yz}$	$\hat{\mathbf{c}}_x y + \hat{\mathbf{c}}_y x$	$\beta, (\alpha\gamma)$
E_u	$\alpha, \beta, \gamma : (\alpha\beta\gamma) : \alpha, \beta, \gamma$	d_{xz}/d_{yz}	$\hat{\mathbf{c}}_z(x, y)$	$\alpha, \beta, \gamma : \gamma, (\alpha\beta) : (\alpha\beta), \gamma$
		$d_{xy}/d_{xz}, d_{xy}/d_{yz}$	$z(\hat{\mathbf{c}}_x, \hat{\mathbf{c}}_y)$	$(\alpha\gamma), \beta : (\alpha\beta\gamma) : (\alpha\gamma), \beta$

a product like $\sin k_x \sin k_y = \frac{1}{2}[\cos(k_x - k_y) - \cos(k_x + k_y)]$ would correspond to a cross-shaped pairing across the nearest-neighbor diagonals, and so on.

Column 4 of Table III shows the nodes associated with each function. The meaning of the symbols used is the following: each of α, β, and γ refers to the normal state Fermi surface sheets (see Fig. 2) and when appearing alone, means that the whole sheet is a nodal surface. Nodal surfaces can be hybridized: For instance, a combination of the β and γ surfaces, noted $(\beta\gamma)$, is visible in the B_{1u} panel of Fig. 3. The $(\alpha\gamma)$ hybridization is seen in the A_{1u} panel of the same figure, and a complete hybridization $(\alpha\beta\gamma)$ in the $E_g(1, 1)$ panel. When a Fermi surface sheet appears in conjunction with $+$, then the intersection of that sheet with horizontal and vertical

axes at 0 and $\pm\pi$ constitute the nodes. The symbols $-$ and $|$ stand for horizontal and vertical lines only. When appearing in conjunction with $\times$, then the intersection of that sheet with diagonals constitutes the nodes. The symbol $\searrow$ stands for the north-west diagonal only. Commas separate different nodal lines or surfaces present. For two-dimensional representations (E_g and E_u), we show the nodes obtained from the (1,0), the (1,1) and the (1, i) combinations, separated by a colon.

E. On the notion of node imposed by symmetry

Column 2 of Table III shows the nodes obtained when combining the different pairing functions of a given representation, with an equal amplitude of 0.25. Thus, this represents the approximate notion of "nodes imposed by symmetry" on each
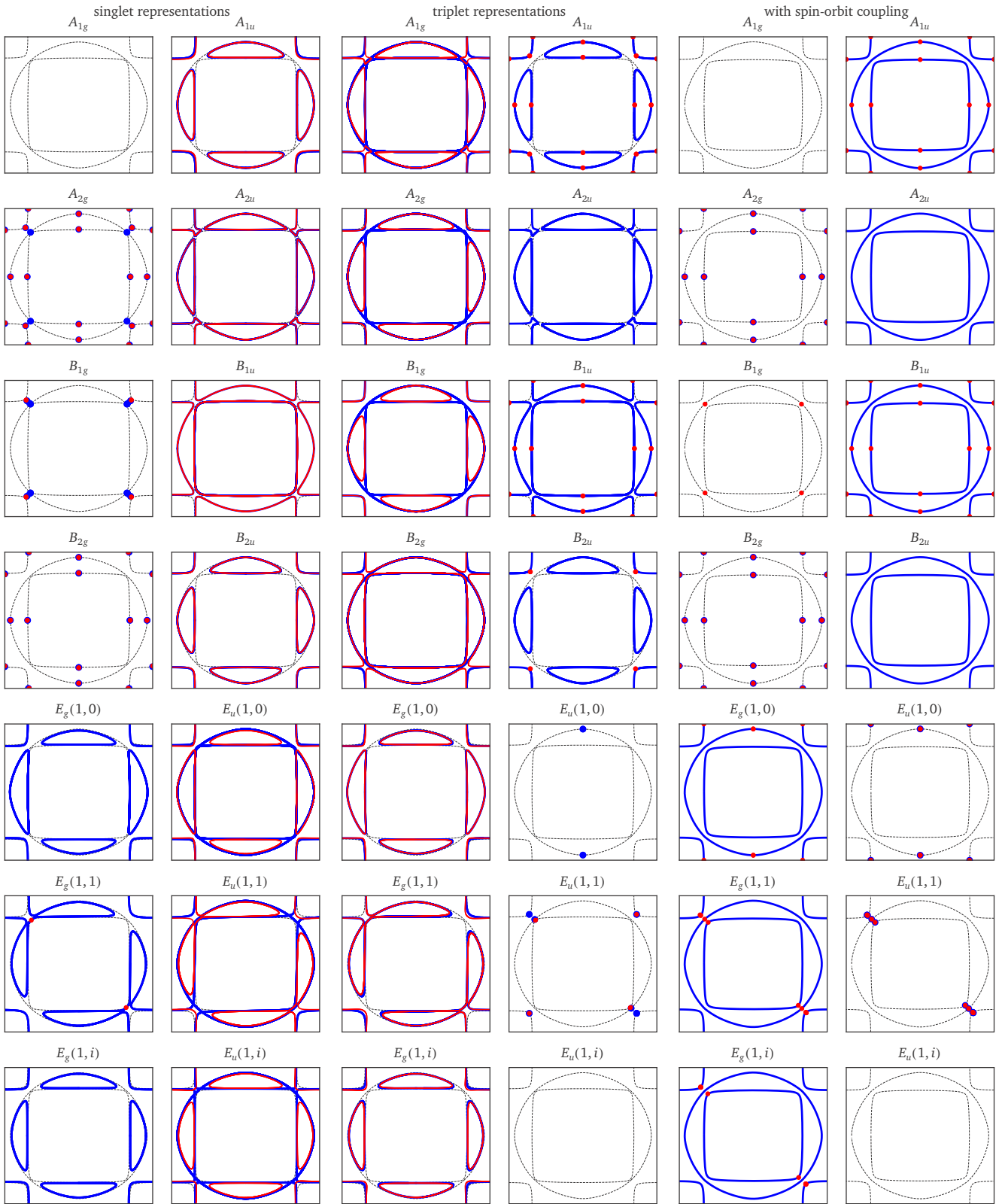
FIG. 3. averaged or typical nodes associated to the different irreps of D_{4h} for $k_z = 0$ (blue) and $k_z = \pi/2$ (red). Each panel covers the full Brillouin zone from $(-\pi, -\pi)$ to (π, π) and the representation label is indicated on top. Left: singlet representations, middle: triplet representations, right: with spin-orbit coupling The normal state Fermi surface is the black dotted line. See text for details.

representation. These are in turn illustrated in the two leftmost columns of Fig. 3. As a rule, the nodes of the combined pairing function in an irrep are the intersection of the nodes of the separate basis functions. The latter may separately have accidental nodes, but those generally disappear when taking linear combinations.

However, strictly speaking, *the notion of symmetry-imposed nodes does not make sense in the case of multiorbital models*, with or without spin-orbit coupling. In the one-band case, whose symmetry classification appears in Table II, a symmetry-imposed node corresponds to a pairing function that vanishes in some direction because it is odd under certain symmetry operations in that irrep. For instance, the pairing function must be odd under a diagonal reflection σ_d in the representation B_{1g} and must accordingly vanish along the diagonals, which is indeed the case of the standard d-wave function $x^2 - y^2$. The pairing function being a scalar, its zeros correspond to nodes. Essentially, the one-band case is simple because translation invariance allows us to express the order parameter as a scalar function of the wave vector $\mathbf{k}$.

In a multiorbital model, the pairing function is a multi-component object: a matrix. That matrix may be odd under a certain symmetry operation, but that does not imply that it must vanish at a fixed point of that operation in momentum space, because the odd character can reside in the orbital part instead of the spatial part. Indeed, the odd character translates into the following transformation property for the pairing function:

$$\Delta_\nu(x, y, z) \rightarrow \Delta'_\nu(x, y, z) = \mathcal{U}(\sigma_d)_{\nu\nu'}\Delta_{\nu'}(y, x, z) \qquad (31)$$

where the index ν labels basis vectors in orbital space and $\mathcal{U}$ the orbital part of the representation. In the B_{1g} representation, we therefore have the condition $\Delta'_\nu(x, y, z) = -\Delta_\nu(x, y, z)$, or $\mathcal{U}(\sigma_d)\Delta(y, x, z) = -\Delta_\nu(x, y, z)$, which translates into $\mathcal{U}(\sigma_d)\Delta(x, x, z) = -\Delta_\nu(x, x, z)$ on the diagonal. In the single-orbital case, $\mathcal{U} = 1$ and that condition implies $\Delta(x, x, z) = 0$. In the multiorbital case, the pairing function may be an eigenvector of $\mathcal{U}$ with eigenvalue -1, and this imposes no condition at all on $\Delta(x, x, z)$. For instance, the pairing function $\hat{\mathbf{a}}_x - \hat{\mathbf{a}}_y$, which is wave-vector independent, belongs to B_{1g}. The matrix $\mathcal{U}$ in that case exchanges a_x and a_y and is equivalent to -1 in orbital space, which leaves an even (here constant) spatial part.

As another example, the interorbital pairing function $\hat{\mathbf{c}}_x x + \hat{\mathbf{c}}_y y$ in representation A_{1u} describes a singlet state that is odd under the reflection σ_z with respect to the xy plane. Indeed, under this reflection, the orbitals d_{xz} and d_{yz} change sign, and so do the components c_x and c_y, while the functions x and y are unaffected. The matrix-valued pairing function then takes the form

$$\Delta(x, y, z) = \begin{pmatrix} 0 & 0 & y \\ 0 & 0 & x \\ -y & -x & 0 \end{pmatrix} \qquad (32)$$

(we ignore spin, which is in a singlet state in this example). The transformation law of that pairing function under σ_z is $\Delta \rightarrow \Delta' = U(\sigma_z)\Delta U(\sigma_z)$, where $U(\sigma_z)$ is given in Table I. Therefore $\Delta' = -\Delta$, as it should be in representation A_{1u}. Accordingly, while that pairing function has nodes (in fact nodal surfaces, since nothing depends on z here), their precise

shape is not imposed by symmetry. In particular they do not coincide with the normal Fermi surfaces but are rather hybridized Fermi surfaces, as illustrated in Fig. 3.

Some of the combined nodes illustrated in Fig. 3 are therefore generic in their character (point or surface) but accidental in their precise shape. Depending on the precise coefficients of the combined pairing function, the precise shape of a hybridized nodal surface may vary slightly.

Table IV lists the triplet pairing functions found using the same procedure. In that case only products of orbital and spatial functions that are antisymmetric under electron exchange were kept. The combined nodes are illustrated in the middle two columns of Fig. 3.

In this figure, we have shown the nodes found on the $k_z = 0$ plane (in blue) and those on the $k_z = \pi/2$ plane (in red). The blue curves on the figure thus correspond to horizontal (more precisely, equatorial) nodal lines. A majority of representations have them. Often nodal lines also occur at $k_z = \pi/2$ but in a hybridized form, hinting at a complex three-dimensional representation of the nodes in those cases. Note that our tight-binding model is still strictly two dimensional. In no case do the generic nodes coincide with the normal state Fermi surfaces. In that sense, superconductivity is never *hidden* in this system, even though it can in many cases be called *gapless*, since the nodes occur at every angle, at least in the absence of spin-orbit coupling.

An important point is that the only two representations that have no nodes are the singlet A_{1g}, which we could commonly call s wave, and the triplet $E_u(1, i)$, which we could call $p_x + ip_y$. This is still true with spin-orbit coupling.

In order to illustrate how these nodes vary upon changing the band parameters, we have plotted the typical nodes for three additional sets of band parameters in Fig. 4. The details of the nodal surfaces change, but the presence of nodal lines along various axes is robust.

F. Spin orbit coupling

In the presence of the spin-orbit coupling ($\kappa \neq 0$), the symmetry is reduced. The spin will transform according to the generators listed in Table I, within a spin representation of D_{4h}, not listed in the character Table II. In particular, within such a spin representation, the fourth power $S(C_4)^4$ is -1, not 1. The tensor product of this spin representation with itself yields symmetric and antisymmetric representations, characterized by the $\mathbf{d}$-vector components. These in turn can be tensored with orbital and spatial representations, provided the overall pairing function is antisymmetric.

Table V lists the possible pairing functions in the presence of spin-orbit coupling. The format used is the same as in Tables III and IV. Note, however, that the Fermi surface of the normal state (the dotted line) is slightly different, because of the added spin-orbit term κ.

The generic nodes of a given representation in the spin-orbit case are generally the intersections of the nodes of the corresponding singlet and triplet representations, although this is not always the case, maybe because the spin-orbit coupling changes the normal-state dispersion as well. Overall, the situation is a bit simpler with spin-orbit coupling: 3D nodal surfaces dot no exist, only equatorial and vertical nodal

TABLE IV. List of triplet pairing functions (no spin-orbit coupling). See Table III and text for an explanation.

Irrep	Combined nodes	Orbital mixing	Pairing function	Nodes
A_{1g}	α, β, γ	d_{xz}/d_{yz} $d_{xy}/d_{xz},\ d_{xy}/d_{yz}$	$\hat{\mathbf{c}}_z xy(x^2-y^2)$ $z(\hat{\mathbf{c}}_x y - \hat{\mathbf{c}}_y x)$	α, β, γ $(\alpha\beta\gamma)$
A_{2g}	α, β, γ	d_{xz}/d_{yz} $d_{xy}/d_{xz},\ d_{xy}/d_{yz}$	$\hat{\mathbf{c}}_z$ $z(\hat{\mathbf{c}}_x x + \hat{\mathbf{c}}_y y)$	α, β, γ $(\alpha\gamma), \beta$
B_{1g}	none	d_{xz}/d_{yz} $d_{xy}/d_{xz},\ d_{xy}/d_{yz}$	$\hat{\mathbf{c}}_z xy$ $z(\hat{\mathbf{c}}_x y + \hat{\mathbf{c}}_y x)$	α, β, γ $(\alpha\gamma), \beta$
B_{2g}	none	d_{xz}/d_{yz} $d_{xy}/d_{xz},\ d_{xy}/d_{yz}$	$\hat{\mathbf{c}}_z(x^2-y^2)$ $z(\hat{\mathbf{c}}_x x - \hat{\mathbf{c}}_y y)$	α, β, γ $\alpha, (\beta\gamma)$
E_g	$\beta, (\alpha\gamma) : (\alpha\beta\gamma) : \beta, (\alpha\gamma)$	d_{xz}/d_{yz} $d_{xy}/d_{xz},\ d_{xy}/d_{yz}$	$\hat{\mathbf{c}}_z z(x, y)$ $(\hat{\mathbf{c}}_x, \hat{\mathbf{c}}_y)$	$\alpha, \beta, \gamma : (\alpha\beta), \gamma : (\alpha\beta), \gamma$ $\beta, (\alpha\gamma) : (\alpha\beta\gamma) : \beta, (\alpha\gamma)$
A_{1u}	$\beta, (\alpha\gamma)$	d_{xy} $d_{xz},\ d_{yz}$ d_{xz}/d_{yz} $d_{xy}/d_{xz},\ d_{xy}/d_{yz}$	$\hat{\mathbf{a}}_z xyz(x^2-y^2)$ $xyz(\hat{\mathbf{a}}_x - \hat{\mathbf{a}}_y)$ $\hat{\mathbf{b}}_z z(x^2-y^2)$ $\hat{\mathbf{b}}_x x + \hat{\mathbf{b}}_y y$	$\alpha, \beta, +\gamma$ $+\alpha, + \times \beta, \gamma$ $+ \times \alpha, + \times \beta, \gamma$ $\beta, (\alpha\gamma)$
A_{2u}	$\alpha, (\beta\gamma)$	d_{xy} $d_{xz},\ d_{yz}$ d_{xz}/d_{yz} $d_{xy}/d_{xz},\ d_{xy}/d_{yz}$	$\hat{\mathbf{a}}_z z$ $z(\hat{\mathbf{a}}_x + \hat{\mathbf{a}}_y)$ $\hat{\mathbf{b}}_z xyz$ $\hat{\mathbf{b}}_x y - \hat{\mathbf{b}}_y x$	α, β γ $+\alpha, +\beta, \gamma$ $(\alpha\beta\gamma)$
B_{1u}	$\alpha, (\beta\gamma)$	d_{xy} $d_{xz},\ d_{yz}$ d_{xz}/d_{yz} $d_{xy}/d_{xz},\ d_{xy}/d_{yz}$	$\hat{\mathbf{a}}_z xyz$ $xyz(\hat{\mathbf{a}}_x + \hat{\mathbf{a}}_y)$ $\hat{\mathbf{b}}_z z$ $\hat{\mathbf{b}}_x x - \hat{\mathbf{b}}_y y$	$\alpha, \beta, +\gamma$ $+\alpha, +\beta, \gamma$ $+\alpha, +\beta, \gamma$ $\alpha, (\beta\gamma)$
B_{2u}	$\beta, (\alpha\gamma)$	d_{xy} $d_{xz},\ d_{yz}$ d_{xz}/d_{yz} $d_{xy}/d_{xz},\ d_{xy}/d_{yz}$	$\hat{\mathbf{a}}_z z(x^2-y^2)$ $z(\hat{\mathbf{a}}_x - \hat{\mathbf{a}}_y)$ $\hat{\mathbf{b}}_z xyz(x^2-y^2)$ $\hat{\mathbf{b}}_x y + \hat{\mathbf{b}}_y x$	$\alpha, \beta, \times\gamma$ $\times\alpha, \times\beta, \gamma$ $+ \times \alpha, + \times \beta, \gamma$ $\beta, (\alpha\gamma)$
E_u	$\|\gamma : \searrow\gamma :$ none	d_{xy} $d_{xz},\ d_{yz}$ d_{xz}/d_{yz} $d_{xy}/d_{xz},\ d_{xy}/d_{yz}$	$\hat{\mathbf{a}}_z(x, y)$ $(\hat{\mathbf{a}}_x x, \hat{\mathbf{a}}_y y)$ $(\hat{\mathbf{a}}_x y, \hat{\mathbf{a}}_y x)$ $\hat{\mathbf{b}}_z(x, y)$ $z(\hat{\mathbf{b}}_x, \hat{\mathbf{b}}_y)$	$\alpha, \beta, \|\gamma : \alpha, \beta, \searrow\gamma : \alpha, \beta$ $+\alpha, +\beta, \gamma : +\alpha, +\beta, \gamma : +\alpha, +\beta, \gamma$ $-\alpha, -\beta, \gamma : \searrow\alpha, \searrow\beta, \gamma : \gamma$ $+\alpha, +\beta, \gamma : +\alpha, +\beta, \gamma : +\alpha, +\beta, \gamma$ $\beta, (\alpha\gamma) : (\alpha\beta\gamma) : (\alpha\gamma), \beta$

lines do. Half of the representations have equatorial nodes. The only representation without nodes are A_{1g} (or s wave) and $E_u(1, i)$ (or $p_x + ip_y$).

G. Uniaxial deformations

Under uniaxial pressure along the x or y axis, Sr$_2$RuO$_4$ will undergo a slight spatial deformation that will reduce its point-group symmetry from D_{4h} to D_{2h}. In this subsection, we outline the changes that this would bring to the classification explained above.

D_{2h} is an Abelian subgroup of D_{4h} and contains half of its elements. Basically, the generator C_4 is no longer a symmetry operation and all group elements obtained from it drop out. The character table of D_{2h} is reproduced in Table VI. The irreps of D_{4h} collapse into the irreps of D_{2h}, as illustrated schematically in Fig. 5.

A similar analysis as done above can be carried out for the D_{2h} symmetry, after adding an anisotropy parameter $\alpha = 0.05$ such that hopping parameters t_1 and t_3 are augmented by α in the x direction and diminished by the same amount in the y direction. This small value of α is sufficient to make the γ-band Fermi surface open, i.e., to bring about a Lifshitz

transition, as observed in experiments [50]. The resulting nodes are illustrated in Fig. 6. The main change from the isotropic case is the disappearance of chiral representations. Thus, the breaking of time-reversal symmetry could only occur by combining different irreps. In particular, the only representation that has no nodes at all is A_{1g} (s wave).

IV. DISCUSSION AND CONCLUSION

The main novelty introduced in this paper is the integration of interorbital pairings, in particular odd-orbital pairings, in the classification of superconductivity for t_{2g} systems. However, at this point we are not in a position to say that this kind of superconductivity is present in Sr$_2$RuO$_4$. Indeed, in addition to suggestions for interorbital pairing [26,27], there are also good arguments to indicate that these kind of pairings should not be favored in the weak-coupling limit [51], even though they are a definite possibility at strong or intermediate coupling. We can still highlight the main differences between interorbital and single-orbital superconductivity, and see how they constrain the interpretation of available experimental data for Sr$_2$RuO$_4$.

TABLE V. List of pairing functions with spin-orbit coupling. See Table III and text for an explanation.

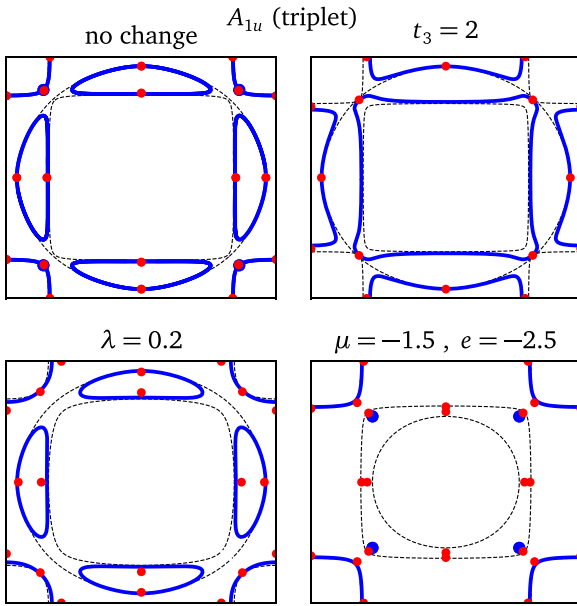| Irrep	Combined nodes	Orbital mixing	Pairing function	Nodes
A_{1g}	none	d_{xy}	$\hat{\mathbf{a}}_z\hat{\mathbf{d}}_0$	α, β
		$d_{xz},\ d_{yz}$	$\hat{\mathbf{d}}_0(\hat{\mathbf{a}}_x+\hat{\mathbf{a}}_y)$	γ
		d_{xz}/d_{yz}	$\hat{\mathbf{c}}_z\hat{\mathbf{d}}_z$	α, β, γ
		$d_{xy}/d_{xz},\ d_{xy}/d_{yz}$	$(\hat{\mathbf{c}}_x\hat{\mathbf{d}}_x-\hat{\mathbf{c}}_y\hat{\mathbf{d}}_y)$	α, β, γ
A_{2g}	$+\alpha, +\beta, +\gamma$	d_{xy}	$\hat{\mathbf{a}}_z\hat{\mathbf{d}}_0 xy(-x^2+y^2)$	$\alpha, \beta, \times+\gamma$
		$d_{xz},\ d_{yz}$	$\hat{\mathbf{d}}_0 xy(-\hat{\mathbf{a}}_x+\hat{\mathbf{a}}_y)$	$+\alpha, +\beta, \gamma$
		d_{xz}/d_{yz}	$\hat{\mathbf{c}}_z z(\hat{\mathbf{d}}_x y+\hat{\mathbf{d}}_y x), \hat{\mathbf{b}}_z\hat{\mathbf{d}}_0(x^2-y^2)$	α, β, γ
		$d_{xy}/d_{xz},\ d_{xy}/d_{yz}$	$\hat{\mathbf{c}}_x\hat{\mathbf{d}}_y+\hat{\mathbf{c}}_y\hat{\mathbf{d}}_x$	α, β, γ
B_{1g}	$\times\gamma$	d_{xy}	$\hat{\mathbf{a}}_z\hat{\mathbf{d}}_0(x^2-y^2)$	$\alpha, \beta, \times\gamma$
		$d_{xz},\ d_{yz}$	$\hat{\mathbf{d}}_0(\hat{\mathbf{a}}_x-\hat{\mathbf{a}}_y)$	γ
		d_{xz}/d_{yz}	$\hat{\mathbf{c}}_z z(\hat{\mathbf{d}}_x x+\hat{\mathbf{d}}_y y), \hat{\mathbf{c}}_z\hat{\mathbf{d}}_z(x^2-y^2)$	α, β, γ
		$d_{xy}/d_{xz},\ d_{xy}/d_{yz}$	$(\hat{\mathbf{c}}_x\hat{\mathbf{d}}_x+\hat{\mathbf{c}}_y\hat{\mathbf{d}}_y)$	α, β, γ
B_{2g}	$+\alpha, +\beta, +\gamma$	d_{xy}	$\hat{\mathbf{a}}_z\hat{\mathbf{d}}_0 xy$	$\alpha, \beta, +\gamma$
		$d_{xz},\ d_{yz}$	$\hat{\mathbf{d}}_0 xy(\hat{\mathbf{a}}_x+\hat{\mathbf{a}}_y)$	$+\alpha, +\beta, \gamma$
		d_{xz}/d_{yz}	$\hat{\mathbf{b}}_z\hat{\mathbf{d}}_0$	α, β, γ
		$d_{xy}/d_{xz},\ d_{xy}/d_{yz}$	$\hat{\mathbf{c}}_x\hat{\mathbf{d}}_y-\hat{\mathbf{c}}_y\hat{\mathbf{d}}_x$	α, β, γ
E_g		d_{xy}	$\hat{\mathbf{a}}_z\hat{\mathbf{d}}_0 z(x,y)$	$\alpha, \beta, |\gamma:\alpha, \beta, \searrow\gamma:\alpha, \beta$
		$d_{xz},\ d_{yz}$	$\hat{\mathbf{d}}_0 z(\hat{\mathbf{a}}_x x, \hat{\mathbf{a}}_y y)$	$-\alpha, -\beta, \gamma:+\alpha, +\beta, \gamma:+\times\alpha, +\beta, \gamma$
	$|\beta, |\gamma:$		$\hat{\mathbf{d}}_0 z(\hat{\mathbf{a}}_x y, \hat{\mathbf{a}}_y x)$	$-\alpha, -\beta, \gamma:\gamma:\times\alpha, \gamma$
	$\searrow\alpha, \searrow\beta, \searrow\gamma$	d_{xz}/d_{yz}	$\hat{\mathbf{c}}_z(\hat{\mathbf{d}}_x, \hat{\mathbf{d}}_y)$	$\alpha, \beta, \gamma:\alpha, \beta, \gamma:\alpha, \beta, \gamma:$
	$\searrow\alpha, \searrow\beta$	$d_{xy}/d_{xz},\ d_{xy}/d_{yz}$	$(-\hat{\mathbf{b}}_y\hat{\mathbf{d}}_0+\hat{\mathbf{c}}_y\hat{\mathbf{d}}_z, \hat{\mathbf{b}}_x\hat{\mathbf{d}}_0+\hat{\mathbf{c}}_x\hat{\mathbf{d}}_z)$	$\alpha, \beta, \gamma:\alpha, \beta, \gamma:\alpha, \beta, \gamma$
			$(\hat{\mathbf{b}}_y\hat{\mathbf{d}}_0+\hat{\mathbf{c}}_y\hat{\mathbf{d}}_z, -\hat{\mathbf{b}}_x\hat{\mathbf{d}}_0+\hat{\mathbf{c}}_x\hat{\mathbf{d}}_z)$	$\alpha, \beta, \gamma:\alpha, \beta, \gamma:\alpha, \beta, \gamma$
A_{1u}	$+\alpha, +\beta, +\gamma$	d_{xy}	$\hat{\mathbf{a}}_z\hat{\mathbf{d}}_0 xyz(x^2-y^2)$	$\alpha, \beta, +\times\gamma$
		$d_{xz},\ d_{yz}$	$\hat{\mathbf{d}}_0 xyz(\hat{\mathbf{a}}_x-\hat{\mathbf{a}}_y)$	$+\alpha, +\beta, \gamma$
		d_{xz}/d_{yz}	$\hat{\mathbf{c}}_z(\hat{\mathbf{d}}_x y+\hat{\mathbf{d}}_y x)$	α, β, γ
		$d_{xy}/d_{xz},\ d_{xy}/d_{yz}$	$z(\hat{\mathbf{c}}_x\hat{\mathbf{d}}_y+\hat{\mathbf{c}}_y\hat{\mathbf{d}}_x), \hat{\mathbf{d}}_z(-\hat{\mathbf{c}}_x y+\hat{\mathbf{c}}_y x), \hat{\mathbf{d}}_0(\hat{\mathbf{b}}_x x+\hat{\mathbf{b}}_y y)$	α, β, γ
A_{2u}	none	d_{xy}	$\hat{\mathbf{a}}_z\hat{\mathbf{d}}_0 z$	α, β
		$d_{xz},\ d_{yz}$	$\hat{\mathbf{d}}_0 z(\hat{\mathbf{a}}_x+\hat{\mathbf{a}}_y)$	γ
		d_{xz}/d_{yz}	$\hat{\mathbf{c}}_z(\hat{\mathbf{d}}_x x-\hat{\mathbf{d}}_y y), \hat{\mathbf{c}}_z\hat{\mathbf{d}}_z z$	α, β, γ
		$d_{xy}/d_{xz},\ d_{xy}/d_{yz}$	$z(\hat{\mathbf{c}}_x\hat{\mathbf{d}}_x-\hat{\mathbf{c}}_y\hat{\mathbf{d}}_y), \hat{\mathbf{d}}_0(\hat{\mathbf{b}}_x y-\hat{\mathbf{b}}_y x), \hat{\mathbf{d}}_z(\hat{\mathbf{c}}_x x+\hat{\mathbf{c}}_y y)$	α, β, γ
B_{1u}	$+\alpha, +\beta, +\gamma$	d_{xy}	$\hat{\mathbf{a}}_z\hat{\mathbf{d}}_0 xyz$	$\alpha, \beta, +\gamma$
		$d_{xz},\ d_{yz}$	$\hat{\mathbf{d}}_0 xyz(\hat{\mathbf{a}}_x+\hat{\mathbf{a}}_y)$	$+\alpha, +\beta, \gamma$
		d_{xz}/d_{yz}	$\hat{\mathbf{c}}_z(-\hat{\mathbf{d}}_x y+\hat{\mathbf{d}}_y x), \hat{\mathbf{b}}_z\hat{\mathbf{d}}_0 z$	α, β, γ
		$d_{xy}/d_{xz},\ d_{xy}/d_{yz}$	$z(\hat{\mathbf{c}}_x\hat{\mathbf{d}}_y-\hat{\mathbf{c}}_y\hat{\mathbf{d}}_x), \hat{\mathbf{d}}_z(\hat{\mathbf{c}}_x y+\hat{\mathbf{c}}_y x), \hat{\mathbf{d}}_0(\hat{\mathbf{b}}_x x-\hat{\mathbf{b}}_y y)$	α, β, γ
B_{2u}	none	d_{xy}	$\hat{\mathbf{a}}_z\hat{\mathbf{d}}_0 z(x^2-y^2)$	$\alpha, \beta, \times\gamma$
		$d_{xz},\ d_{yz}$	$\hat{\mathbf{d}}_0 z(\hat{\mathbf{a}}_x-\hat{\mathbf{a}}_y)$	γ
		d_{xz}/d_{yz}	$\hat{\mathbf{c}}_z(\hat{\mathbf{d}}_x x+\hat{\mathbf{d}}_y y)$	α, β, γ
		$d_{xy}/d_{xz},\ d_{xy}/d_{yz}$	$z(\hat{\mathbf{c}}_x\hat{\mathbf{d}}_x+\hat{\mathbf{c}}_y\hat{\mathbf{d}}_y), \hat{\mathbf{d}}_0(\hat{\mathbf{b}}_x y+\hat{\mathbf{b}}_y x), \hat{\mathbf{d}}_z(\hat{\mathbf{c}}_x x-\hat{\mathbf{c}}_y y)$	α, β, γ
E_u		d_{xy}	$\hat{\mathbf{a}}_z\hat{\mathbf{d}}_0(x,y)$	$\alpha, \beta, |\gamma:\alpha, \beta, \searrow\gamma:\alpha, \beta$
		$d_{xz},\ d_{yz}$	$\hat{\mathbf{d}}_0(\hat{\mathbf{a}}_x x, \hat{\mathbf{a}}_y y)$	$+\alpha, +\beta, \gamma:+\alpha, +\beta, \gamma:+\alpha, +\beta, \gamma$
			$\hat{\mathbf{d}}_0(\hat{\mathbf{a}}_x y, \hat{\mathbf{a}}_y x)$	$-\alpha, -\beta, \gamma:\gamma:\times\alpha, \gamma$
		d_{xz}/d_{yz}	$\hat{\mathbf{c}}_z z(\hat{\mathbf{d}}_x, \hat{\mathbf{d}}_y), (\hat{\mathbf{b}}_z\hat{\mathbf{d}}_0-\hat{\mathbf{c}}_z\hat{\mathbf{d}}_z)(x,y), (\hat{\mathbf{b}}_z\hat{\mathbf{d}}_0+\hat{\mathbf{c}}_z\hat{\mathbf{d}}_z)(x,y)$	$\alpha, \beta, \gamma:\alpha, \beta, \gamma:\alpha, \beta, \gamma$
	$|\beta, |\gamma:$	$d_{xy}/d_{xz},\ d_{xy}/d_{yz}$	$(\hat{\mathbf{c}}_y x(\hat{\mathbf{d}}_x-i\hat{\mathbf{d}}_y), \hat{\mathbf{c}}_y y(\hat{\mathbf{d}}_x+i\hat{\mathbf{d}}_y))$	$\alpha, \beta, \gamma:\alpha, \beta, \gamma:\alpha, \beta, \gamma$
	$\searrow\alpha, \searrow\beta, \searrow\gamma:$		$(\hat{\mathbf{c}}_y y(\hat{\mathbf{d}}_x-i\hat{\mathbf{d}}_y), \hat{\mathbf{c}}_y x(\hat{\mathbf{d}}_x+i\hat{\mathbf{d}}_y))$	$\alpha, \beta, \gamma:\alpha, \beta, \gamma:\alpha, \beta, \gamma$
	none		$z(\hat{\mathbf{b}}_y\hat{\mathbf{d}}_0-\hat{\mathbf{c}}_y\hat{\mathbf{d}}_z, \hat{\mathbf{b}}_x\hat{\mathbf{d}}_0+\hat{\mathbf{c}}_x\hat{\mathbf{d}}_z)$	$\alpha, \beta, \gamma:\alpha, \beta, \gamma:\alpha, \beta, \gamma$
			$z(\hat{\mathbf{b}}_y\hat{\mathbf{d}}_0+\hat{\mathbf{c}}_y\hat{\mathbf{d}}_z, \hat{\mathbf{b}}_x\hat{\mathbf{d}}_0-\hat{\mathbf{c}}_x\hat{\mathbf{d}}_z)$	$\alpha, \beta, \gamma:\alpha, \beta, \gamma:\alpha, \beta, \gamma$
			$(\hat{\mathbf{c}}_y x(\hat{\mathbf{d}}_x+i\hat{\mathbf{d}}_y), \hat{\mathbf{c}}_x y(-\hat{\mathbf{d}}_x+i\hat{\mathbf{d}}_y))$	$\alpha, \beta, \gamma:\alpha, \beta, \gamma:\alpha, \beta, \gamma$
			$(\hat{\mathbf{c}}_y y(\hat{\mathbf{d}}_x+i\hat{\mathbf{d}}_y), \hat{\mathbf{c}}_x x(-\hat{\mathbf{d}}_x+i\hat{\mathbf{d}}_y))$	$\alpha, \beta, \gamma:\alpha, \beta, \gamma:\alpha, \beta, \gamma$

FIG. 4. Averaged or typical nodes associated to the triplet representation A_{1u} but with different band parameters. Top left: No change in the parameters. Other panels are obtained by changing the parameters as indicated on top of each panel. In particular, the bottom right panel corresponds to a drastic change in band parameters incompatible with Sr_2RuO_4. Again, the $k_z = 0$ nodes are in blue (including equatorial nodes), and the $k_z = \pi/2$ vertical nodal lines are shown as red dots. The normal state Fermi surface is the black dotted line.

A. Singlet vs triplet superconductivity

An odd orbital part for the superconducting order parameter (i.e., involving the **c** vector) allows the combination of singlet and odd parity, or triplet and even parity order parameters. This contrasts with the single-orbital case where singlet and triplet, respectively, imply even and odd parity. Here, both singlet and triplet can be associated with any e-type or u-type representation. In the presence of spin-orbit coupling, this implies that there is no clear distinction between singlet and triplet and that a combination of both is possible in general, as seen in Table V. Some studies [52,53] have suggested the possibility of combining singlet and triplet order parameters in Sr_2RuO_4 due to strong spin-orbit coupling. Our analysis shows that the only way to achieve such combinations within the same irreducible representation is through odd orbital pairing.

Also, recent Knight shift measurements [9] show a substantial drop in the spin susceptibility across T_c, with or

TABLE VI. Character table of D_{2h}.

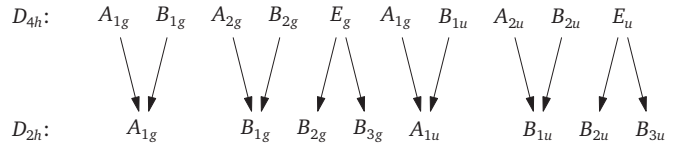|	E	C_{2z}	C_{2y}	C_{2x}	i	σ_z	σ_y	σ_x
A_g	1	1	1	1	1	1	1	1
B_{1g}	1	1	−1	−1	1	1	−1	−1
B_{2g}	1	−1	1	−1	1	−1	1	−1
B_{3g}	1	−1	−1	1	1	−1	−1	1
A_{1u}	1	1	1	1	−1	−1	−1	−1
B_{1u}	1	1	−1	−1	−1	−1	1	1
B_{2u}	1	−1	1	−1	−1	1	−1	1
B_{3u}	1	−1	−1	1	−1	1	1	−1

FIG. 5. Branching of the irreducible representations of D_{4h} (top) into those of D_{2h} (bottom).

without uniaxial strain. This seems to rule out any pairing function with an important $\hat{\mathbf{d}}_z$ component in the spin sector. However, this does not rule out any of the representations of Table V, since the $\hat{\mathbf{d}}_z$ components are never alone in those.

B. Odd vs even superconductivity

As can be seen from Table I, the inversion operation $i = \sigma_x \sigma_y \sigma_z$ has no effect on the orbitals, and therefore on the **a**, **b**, and **c** vectors. This implies that all states within an irrep have the same spatial parity. In particular, all g-type representations are even and all u-type representations are odd. Josephson interferometry experiments [6–8] have suggested that the order parameter of Sr_2RuO_4 has odd parity. If this were true, it would eliminate all the g-type representations.

C. Broken time-reversal symmetry

Broken time-reversal symmetry, supported by muon spin resonance [10] and polar Kerr effect [11] experiments, can only occur in our paradigm within two-dimensional irreps (E_g and E_u). However, the absence of splitting of the superconducting transition when applying strain [18–20] seems to exclude that possibility. We are facing a contradiction that cannot be resolved without abandoning the single phase transition hypothesis; the possibility of interorbital pairing is of no help here.

D. Nodes and the density of states

One of the main motivations of this work was to predict typical nodal structures from symmetry considerations. We have seen that the notion of nodes imposed by symmetry is not strictly valid when many orbitals are involved in the superconducting state. However, there are typical nodes that can be observed in a given irreducible representation, and they are shown in Fig. 3. There is contradicting evidence for both vertical nodal lines [13,14,16] and horizontal nodal lines [15] in Sr_2RuO_4.

However, nodal *surfaces* would lead to a finite density of states at the Fermi level within the superconducting state, which seems excluded [14]. Simple single-orbital pairing functions involving only $\hat{\mathbf{a}}_z$, or a combination of $\hat{\mathbf{a}}_x$ and $\hat{\mathbf{a}}_y$, would lead to nodal surfaces coinciding with the Fermi surfaces of the bands not involved in pairing. It is likely, however, that interactions would cause superconductivity to have components in every band. Figure 3 shows that u-type singlet representations and g-type triplet representations have nodal surfaces. These disappear when spin-orbit coupling is important.

If we exclude two-dimensional representations, keeping nodal vertical and horizontal nodal lines would tend to favor representations A_{1u} and B_{1u} if spin-orbit coupling is important.
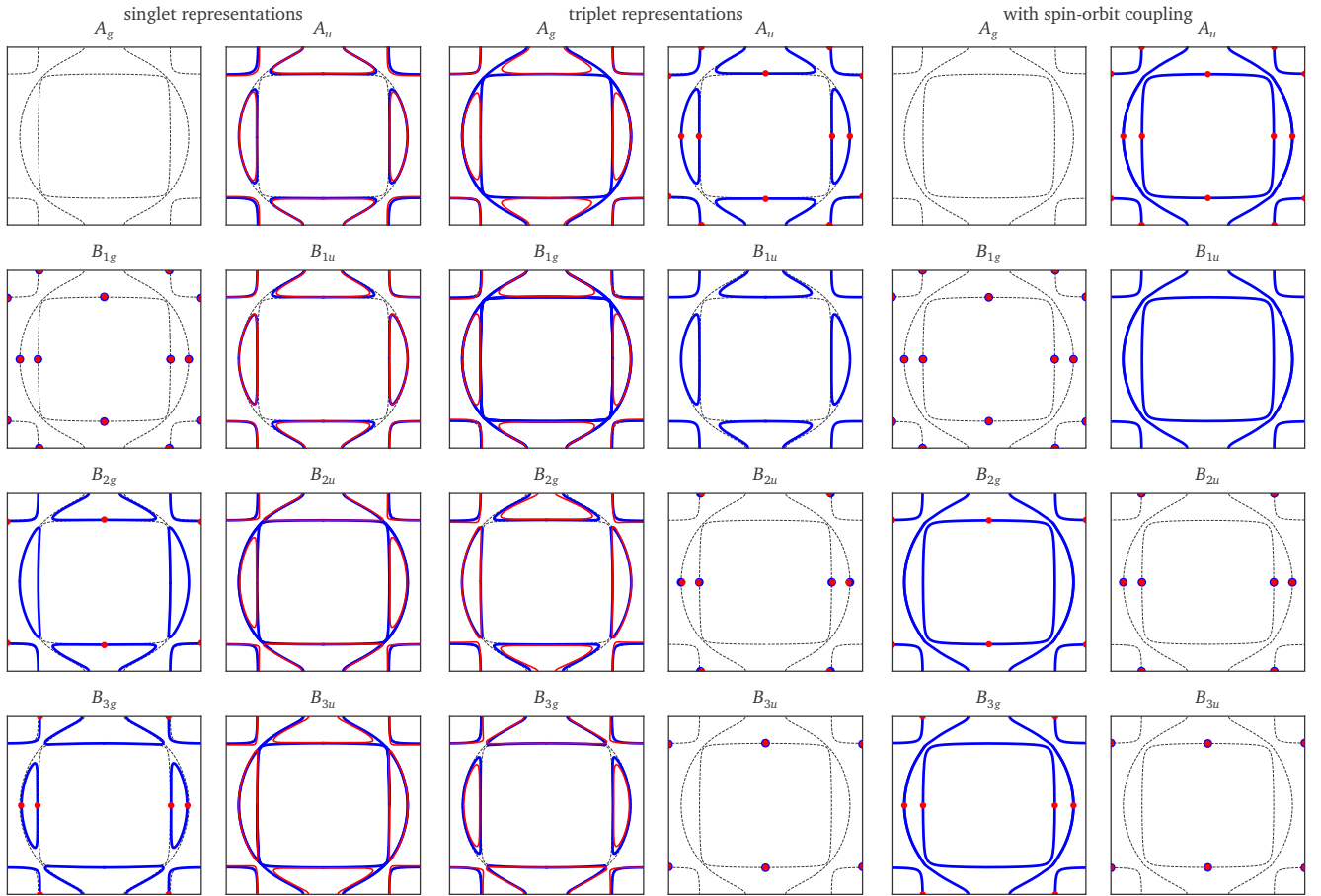
FIG. 6. Averaged or typical nodes associated to the different irreducible representations of D_{2h} for $k_z = 0$ (blue) and $k_z = \pi/2$ (red). Each panel covers the full Brillouin zone from $(-\pi, -\pi)$ to (π, π) and the representation label is indicated on top. Left: singlet representations, middle: triplet representations, right: with spin-orbit coupling. The normal state Fermi surface is the black dotted line.

Incidently, both of these are odd under inversion, which is also supported by observations [6].

From a strongly interacting perspective, it makes sense to seek real-space pairing along the same bonds as the most important hopping terms. Therefore we are led to favor the lowest possible degree in pairing functions, as they correspond to the shortest ranges, and to exclude pairing functions in the z direction. It is, however, difficult to meet this requirement while considering a gap with horizontal nodes, with or without interorbital pairing. For instance, the spin-orbit irreps A_{1u} and B_{2u} have horizontal and vertical nodes, no nodal surfaces, but the simplest pairing functions belonging to these representations (from Table V) involve interorbital, nearest-neighbor pairing, which does not correspond to hopping terms of the model studied. On the other hand, the spin-orbit E_g representations also have the correct nodal content, have constant interorbital pairing functions, and even allow for a broken time-reversal solution $[E_g(1, i)]$. Furthermore, these nodes are preserved even as uniaxial pressure is applied (see Fig. 6 under B_{2g} and B_{3g}). However, as mentioned above, the absence of

transition splitting when applying uniaxial pressure does not favor representations of this type, and they are not odd under inversion.

Let us remark that our results can easily be applied to other t_{2g} systems with D_{4h} symmetry. The precise values of the hopping terms are not important in the classification we presented, although some fine details about the shape of the nodes will vary, as illustrated in Fig. 4.

Note Added. Recently, we became aware of other current work dealing with the same issues [54,55].

[1] A. P. Mackenzie and Y. Maeno, The superconductivity of Sr$_2$RuO$_4$ and the physics of spin-triplet pairing, Rev. Mod. Phys. **75**, 657 (2003).

[2] Y. Liu and Z.-Q. Mao, Unconventional superconductivity in Sr$_2$RuO$_4$, Physica C **514**, 339 (2015).

[3] A. P. Mackenzie, T. Scaffidi, C. W. Hicks, and Y. Maeno, Even odder after twenty-three years: the superconducting order parameter puzzle of Sr_2RuO_4, npj Quantum Mater. **2**, 40 (2017).

[4] K. Ishida, H. Mukuda, Y. Kitaoka, K. Asayama, Z. Q. Mao, Y. Mori, and Y. Maeno, Spin-triplet superconductivity in Sr_2RuO_4 identified by 17o knight shift, Nature (London) **396**, 658 (1998).

[5] J. A. Duffy, S. M. Hayden, Y. Maeno, Z. Mao, J. Kulda, and G. J. McIntyre, Polarized-Neutron Scattering Study of the Cooper-Pair Moment in Sr_2RuO_4, Phys. Rev. Lett. **85**, 5412 (2000).

[6] K. D. Nelson, Z. Q. Mao, Y. Maeno, and Y. Liu, Odd-parity superconductivity in Sr_2RuO_4, Science **306**, 1151 (2004).

[7] F. Laube, G. Goll, H. v. Löhneysen, M. Fogelström, and F. Lichtenberg, Spin-Triplet Superconductivity in Sr_2RuO_4 Probed by Andreev Reflection, Phys. Rev. Lett. **84**, 1595 (2000).

[8] Y. Liu, Phase-sensitive-measurement determination of odd-parity, spin-triplet superconductivity in Sr_2RuO_4, New J. Phys. **12**, 075001 (2010).

[9] A. Pustogow, Y. Luo, A. Chronister, Y. S. Su, D. A. Sokolov, F. Jerzembeck, A. P. Mackenzie, C. W. Hicks, N. Kikugawa, S. Raghu, E. D. Bauer, and S. E. Brown, Pronounced drop of ^{17}O NMR Knight shift in superconducting state of Sr_2RuO_4, Nature (London) **574**, 72 (2019).

[10] G. M. Luke, Y. Fudamoto, K. M. Kojima, M. I. Larkin, J. Merrin, B. Nachumi, Y. J. Uemura, Y. Maeno, Z. Q. Mao, Y. Mori, H. Nakamura, and M. Sigrist, Time-reversal symmetry-breaking superconductivity in Sr_2RuO_4, Nature (London) **394**, 558 (1998).

[11] J. Xia, Y. Maeno, P. T. Beyersdorf, M. M. Fejer, and A. Kapitulnik, High Resolution Polar Kerr Effect Measurements of Sr_2RuO_4: Evidence for Broken Time-Reversal Symmetry in the Superconducting State, Phys. Rev. Lett. **97**, 167002 (2006).

[12] T. M. Rice and M. Sigrist, Sr_2RuO_4: an electronic analog of ^3He? J. Phys.: Condens. Matter **7**, L643 (1995).

[13] S. NishiZaki, Y. Maeno, and Z. Mao, Changes in the superconducting state of Sr_2RuO_4 under magnetic fields probed by specific heat, J. Phys. Soc. Jpn. **69**, 572 (2000).

[14] E. Hassinger, P. Bourgeois-Hope, H. Taniguchi, S. R. de Cotret, G. Grissonnanche, M. S. Anwar, Y. Maeno, N. Doiron-Leyraud, and L. Taillefer, Vertical Line Nodes in the Superconducting Gap Structure of Sr_2RuO_4, Phys. Rev. X **7**, 011032 (2017).

[15] S. Kittaka, S. Nakamura, T. Sakakibara, N. Kikugawa, T. Terashima, S. Uji, D. A. Sokolov, A. P. Mackenzie, K. Irie, Y. Tsutsumi, K. Suzuki, and K. Machida, Searching for gap zeros in Sr_2RuO_4 via field-angle-dependent specific-heat measurement, J. Phys. Soc. Jpn. **87**, 093703 (2018).

[16] C. Lupien, W. A. MacFarlane, C. Proust, L. Taillefer, Z. Q. Mao, and Y. Maeno, Ultrasound Attenuation in Sr_2RuO_4: An Angle-Resolved Study of the Superconducting Gap Function, Phys. Rev. Lett. **86**, 5986 (2001).

[17] S. Kittaka, A. Kasahara, T. Sakakibara, D. Shibata, S. Yonezawa, Y. Maeno, K. Tenya, and K. Machida, Sharp magnetization jump at the first-order superconducting transition in Sr_2RuO_4, Phys. Rev. B **90**, 220502(R) (2014).

[18] C. W. Hicks, D. O. Brodsky, E. A. Yelland, A. S. Gibbs, J. A. N. Bruin, M. E. Barber, S. D. Edkins, K. Nishimura, S. Yonezawa, Y. Maeno, and A. P. Mackenzie, Strong increase of T_3 of Sr_2RuO_4 under both tensile and compressive strain, Science **344**, 283 (2014).

[19] A. Steppke, L. Zhao, M. E. Barber, T. Scaffidi, F. Jerzembeck, H. Rosner, A. S. Gibbs, Y. Maeno, S. H. Simon, A. P. Mackenzie, and C. W. Hicks, Strong peak in T_3 of Sr_2RuO_4 under uniaxial pressure, Science **355**, eaaf9398 (2017).

[20] C. A. Watson, A. S. Gibbs, A. P. Mackenzie, C. W. Hicks, and K. A. Moler, Micron-scale measurements of low anisotropic strain response of local T_c in Sr_2RuO_4, Phys. Rev. B **98**, 094521 (2018).

[21] Y. Maeno, H. Hashimoto, K. Yoshida, S. Nishizaki, T. Fujita, J. G. Bednorz, and F. Lichtenberg, Superconductivity in a layered perovskite without copper, Nature (London) **372**, 532 (1994).

[22] D. F. Agterberg, T. M. Rice, and M. Sigrist, Orbital Dependent Superconductivity in Sr_2RuO_4, Phys. Rev. Lett. **78**, 3374 (1997).

[23] I. I. Mazin and D. J. Singh, Ferromagnetic Spin Fluctuation Induced Superconductivity in Sr_2RuO_4, Phys. Rev. Lett. **79**, 733 (1997).

[24] S. Raghu, A. Kapitulnik, and S. A. Kivelson, Hidden Quasi-One-Dimensional Superconductivity in Sr_2RuO_4, Phys. Rev. Lett. **105**, 136401 (2010).

[25] T. Scaffidi, J. C. Romers, and S. H. Simon, Pairing symmetry and dominant band in Sr_2RuO_4, Phys. Rev. B **89**, 220510(R) (2014).

[26] C. M. Puetter and H.-Y. Kee, Identifying spin-triplet pairing in spin-orbit coupled multi-band superconductors, Europhys. Lett. **98**, 27010 (2012).

[27] O. Gingras, R. Nourafkan, A.-M. S. Tremblay, and M. Côté, Superconducting Symmetries of Sr_2RuO_4 from First-Principles Electronic Structure, Phys. Rev. Lett. **123**, 217005 (2019).

[28] Y. Yanase, S. Takamatsu, and M. Udagawa, Spin–orbit coupling and multiple phases in spin-triplet superconductor Sr_2RuO_4, J. Phys. Soc. Jpn. **83**, 061019 (2014).

[29] S. Acharya, M. S. Laad, D. Dey, T. Maitra, and A. Taraphder, First-principles correlated approach to the normal state of strontium ruthenate, Sci. Rep. **7**, 43033 (2017).

[30] M. W. Haverkort, I. S. Elfimov, L. H. Tjeng, G. A. Sawatzky, and A. Damascelli, Strong Spin-Orbit Coupling Effects on the Fermi Surface of Sr_2RuO_4 and Sr_2RhO_4, Phys. Rev. Lett. **101**, 026406 (2008).

[31] K. K. Ng and M. Sigrist, The role of spin-orbit coupling for the superconducting state in Sr_2RuO_4, Europhys. Lett. **49**, 473 (2000).

[32] H. Iwasawa, Y. Yoshida, I. Hase, S. Koikegami, H. Hayashi, J. Jiang, K. Shimada, H. Namatame, M. Taniguchi, and Y. Aiura, Interplay Among Coulomb Interaction, Spin-Orbit Interaction, and Multiple Electron-Boson Interactions in Sr_2RuO_4, Phys. Rev. Lett. **105**, 226406 (2010).

[33] V. B. Zabolotnyy, D. V. Evtushinsky, A. A. Kordyuk, T. K. Kim, E. Carleschi, B. P. Doyle, R. Fittipaldi, M. Cuoco, A. Vecchione, and S. V. Borisenko, Renormalized band structure of Sr_2RuO_4: A quasiparticle tight-binding approach, J. Electron Spectrosc. Relat. Phenom. **191**, 48 (2013).

[34] A. Tamai, M. Zingl, E. Rozbicki, E. Cappelli, S. Ricco, A. de la Torre, S. McKeown Walker, F. Y. Bruno, P. D. C. King, W. Meevasana, M. Shi, M. Radovic, N. C. Plumb, A. S. Gibbs, A. P. Mackenzie, C. Berthod, H. Strand, M. Kim, A. Georges, and F. Baumberger, High-Resolution Photoemission on Sr_2RuO_4 Reveals Correlation-Enhanced Effective Spin-Orbit Coupling

and Dominantly Local Self-Energies, Phys. Rev. X **9**, 021048 (2019).

[35] M. Sigrist and M. E. Zhitomirsky, Pairing symmetry of the superconductor Sr_2RuO_4, J. Phys. Soc. Jpn. **65**, 3452 (1996).

[36] M. Sigrist, D. Agterberg, A. Furusaki, C. Honerkamp, K. K. Ng, T. M. Rice, and M. E. Zhitomirsky, Phenomenology of the superconducting state in Sr_2RuO_4, Physica C: Superconductivity **317-318**, 134 (1999).

[37] A. M. Black-Schaffer and A. V. Balatsky, Odd-frequency superconducting pairing in multiband superconductors, Phys. Rev. B **88**, 104514 (2013).

[38] R. M. Geilhufe and A. V. Balatsky, Symmetry analysis of odd- and even-frequency superconducting gap symmetries for time-reversal symmetric interactions, Phys. Rev. B **97**, 024507 (2018).

[39] J. F. Annett, Symmetry of the order parameter for high-temperature superconductivity, Adv. Phys. **39**, 83 (1990).

[40] M. Sigrist and K. Ueda, Phenomenological theory of unconventional superconductivity, Rev. Mod. Phys. **63**, 239 (1991).

[41] S.-O. Kaba, *Symétrie du paramètre d'ordre supraconducteur dans le ruthénate de strontium*, MSc(Université de Sherbrooke, Sherbrooke, QC, Canada, 2018).

[42] C. Noce and T. Xiang, A tight-binding model for Sr_2RuO_4, Physica C: Superconductivity **282-287**, 1713 (1997), proceedings of the International Conference on Materials and Mechanisms of Superconductivity High Temperature Superconductors V.

[43] C. Bergemann, A. P. Mackenzie, S. R. Julian, D. Forsythe, and E. Ohmichi, Quasi-two-dimensional fermi liquid properties of the unconventional superconductor Sr_2RuO_4, Adv. Phys. **52**, 639 (2003).

[44] Q. H. Wang, C. Platt, Y. Yang, C. Honerkamp, F. C. Zhang, W. Hanke, T. M. Rice, and R. Thomale, Theory of superconductivity in a three-orbital model of Sr_2RuO_4, Europhys. Lett. **104**, 17013 (2013).

[45] J. Mravlje, M. Aichhorn, T. Miyake, K. Haule, G. Kotliar, and A. Georges, Coherence-Incoherence Crossover and the Mass-Renormalization Puzzles in Sr_2RuO_4, Phys. Rev. Lett. **106**, 096401 (2011).

[46] I. I. Mazin and D. J. Singh, Competitions in Layered Ruthenates: Ferromagnetism Versus Antiferromagnetism and Triplet Versus Singlet Pairing, Phys. Rev. Lett. **82**, 4324 (1999).

[47] A. Liebsch and A. Lichtenstein, Photoemission Quasiparticle Spectra of Sr_2RuO_4, Phys. Rev. Lett. **84**, 1591 (2000).

[48] M. Tsuchiizu, Y. Yamakawa, S. Onari, Y. Ohno, and H. Kontani, Spin-triplet superconductivity in Sr_2RuO_4 due to orbital and spin fluctuations: Analyses by two-dimensional renormalization group theory and self-consistent vertex-correction method, Phys. Rev. B **91**, 155103 (2015).

[49] Note here that we did not invert the spin quantum number in the second half of the Nambu spinor. This is matter of convenience and amounts to changing the order of the components compared to the usual convention.

[50] V. Sunko, E. Abarca Morales, I. Marković, M. E. Barber, D. Milosavljević, F. Mazzola, D. A. Sokolov, N. Kikugawa, C. Cacho, P. Dudin, H. Rosner, C. W. Hicks, P. D. C. King, and A. P. Mackenzie, Direct Observation of a Uniaxial Stress-driven Lifshitz Transition in Sr_2RuO_4, arXiv:1903.09581.

[51] A. Ramires and M. Sigrist, Identifying detrimental effects for multiorbital superconductivity: Application to Sr_2RuO_4, Phys. Rev. B **94**, 104501 (2016).

[52] C. N. Veenstra, Z.-H. Zhu, M. Raichle, B. M. Ludbrook, A. Nicolaou, B. Slomski, G. Landolt, S. Kittaka, Y. Maeno, J. H. Dil *et al.*, Spin-Orbital Entanglement and the Breakdown of Singlets and Triplets in Sr_2RuO_4 Revealed by Spin-and Angle-Resolved Photoemission Spectroscopy, Phys. Rev. Lett. **112**, 127002 (2014).

[53] G. Zhang, E. Gorelov, E. Sarvestani, and E. Pavarini, Fermi Surface of Sr_2RuO_4: Spin-Orbit and Anisotropic Coulomb Interaction Effects, Phys. Rev. Lett. **116**, 106402 (2016).

[54] A. Ramires and M. Sigrist, The superconducting order parameter of Sr_2RuO_4: A microscopic perspective, Phys. Rev. B **100**, 104501 (2019).

[55] W. Huang, Y. Zhou, and H. Yao, Exotic Cooper pairing in multi-orbital models of Sr_2RuO_4, Phys. Rev. B **100**, 134506 (2019).